

# Systematic Investigation of Fuel Efficiency Restoration During Engine Overhaul

A thesis accepted by the Faculty of Aerospace Engineering and Geodesy of the  
Universität Stuttgart in partial fulfillment of the requirements for the degree of  
Doctor of Engineering Sciences (Dr.-Ing.)

by

**Dipl.-Ing. Jonathan Sebastian Kuschke**

born in Celle, Germany

Main referee:	Prof. Dr.-Ing. Stephan Staudacher
Co-referee:	Prof. Dr.-Ing. Roland Fiola
Date of the oral examination:	May 29th, 2015

Institute of Aircraft Propulsion Systems of the Universität Stuttgart  
2015



In dedication to my greatest personal  
role model, my grandfather.



# Acknowledgements

The present doctoral dissertation originates from my time as an employee at MTU Aero Engines. The company and its subsidiary MTU Maintenance Hannover have permitted this work by providing me with available engine data, as well as access to their engine specific IT-tools. For this and the possibility to publish my results, I am grateful.

I thank Prof. Dr.-Ing. Stephan Staudacher for both his personal supervision of this dissertation and many valuable insights and discussions. To Prof. Dr.-Ing. Roland Fiola, I express my thanks for his interest in this dissertation and for co-refereeing it.

A very special thanks goes to Mr. André Kando and Dr.-Ing. Holger Schulte of MTU Aero Engines. Their personal mentoring of my research activity and this document have been highly valuable. It has been the foundation for both a sensible course and the output quality of this doctoral project.

Most importantly, I want to thank my family, my girl-friend Edith Jacob-Wendler and friends for their support during both the time it took for this dissertation to finish and all that came before. My particular gratitude goes to my mother, Paulina Pöpperl, who has supported me and believed in me unconditionally for more than thirty years. Without this, I would not have made it this far.

Munich, May of 2015

Jonathan Kuschke



# Contents

List of Figures	iii
List of Tables	v
Nomenclature	vii
Abstract	xiii
Kurzfassung	xv
<b>1 Introduction</b>	<b>1</b>
<b>2 Existing Methods</b>	<b>3</b>
<b>3 Project Objective and Proceeding</b>	<b>7</b>
<b>4 Assessment of the Overhaul Workscope</b>	<b>11</b>
4.1 Operation-Induced Feature Changes . . . . .	11
4.2 Modelling Overhaul-Induced Feature Restoration . . . . .	13
4.3 Regard of the Level of Detail . . . . .	15
4.4 Identification of Performance-Relevant Features . . . . .	16
<b>5 Assessment of the Overhaul Effect</b>	<b>19</b>
5.1 Demonstration of the Assessment Methodology . . . . .	20
5.1.1 Modelling of Non-Observable Turbo Components . . . . .	22
5.1.2 Modelling of Secondary Effects . . . . .	24
5.2 Measurement Uncertainties . . . . .	29
5.2.1 Description of On-Wing Measurement Process . . . . .	29
5.2.2 Field Data-Based Assessment of Random Measurement Uncertainty . . . . .	31
5.2.3 Field Data-Based Assessment of the Stochastic Part of the Remaining Systematic Measurement Uncertainty . . . . .	37

5.2.4	Requirement-Based Assessment of Maximum Permissible Mach Number Measurement Uncertainty . . . . .	38
5.2.5	Test Cell Measurements . . . . .	39
5.3	Model Uncertainties . . . . .	40
5.3.1	Fuel Heating Value . . . . .	40
5.3.2	Exhaust Nozzle Exit Area . . . . .	41
5.3.3	Thrust Reverser Leakage . . . . .	41
5.3.4	Water Content of the Ambient Air . . . . .	42
5.3.5	Booster and HPT Capacity Recovery . . . . .	43
5.3.6	Secondary Air System . . . . .	43
5.3.7	Engine Settings . . . . .	45
5.4	Simulation of Performance Recovery Analysis Uncertainty . . . . .	45
5.4.1	Monte Carlo Simulation . . . . .	45
5.4.2	Assessment of Total Analysis Uncertainty . . . . .	48
<b>6</b>	<b>Correlation of Overhaul Workscope and Effect</b>	<b>53</b>
6.1	Correlation Process . . . . .	53
6.2	Validation of the Correlation . . . . .	55
6.2.1	Assessment of the Input Data . . . . .	56
6.2.2	Assessment of the Correlated Model . . . . .	57
6.3	Application of the Methodology . . . . .	60
<b>7</b>	<b>Concluding Discussion</b>	<b>65</b>
7.1	Summary . . . . .	65
7.2	Outlook . . . . .	66
	<b>Bibliography</b>	<b>69</b>
	<b>Appendix A</b>	<b>77</b>
A.1	Ratio of Pressure Measurements Uncertainties . . . . .	77
A.2	Uncertainties of Performance Recovery Analysis . . . . .	78
	<b>Curriculum Vitae</b>	<b>81</b>



# List of Figures

1.1	Generalized SFC deterioration . . . . .	2
3.1	Scheme of the project architecture . . . . .	8
4.1	Schematic representation of probabilistic hardware feature evolution . . . . .	13
5.1	Evolution of monitored gas path measurements . . . . .	19
5.2	Setup of the statistical model for HPT capacity recovery . . . . .	24
5.3	Nozzle discharge coefficient change due to Reynolds number variation . . . . .	26
5.4	Linear clearance model for HPC efficiency based on field data . . . . .	28
5.5	Pressure measurement chain of production pressure instrumentation . . . . .	29
5.6	Deviation of left wing and right wing EGT before filtering . . . . .	31
5.7	Deviation of left wing and right wing EGT after filtering . . . . .	32
5.8	Smooth curve deviation of left wing and right wing EGT after filtering . . . . .	33
5.9	Measurement uncertainty comparison I . . . . .	35
5.10	Measurement uncertainty comparison II . . . . .	36
5.11	Distribution of FHV for airline operation . . . . .	41
5.12	Monte Carlo Simulation setup for random measurement uncertainty . . . . .	46
5.13	Monte Carlo Simulation setup for nozzle area variation . . . . .	47
5.14	$U_{95}$ for analysed HPC efficiency recovery . . . . .	51
5.15	$U_{95}$ for analysed HPT efficiency recovery I . . . . .	52
6.1	Scheme of a cross-validation loop using the leave one out algorithm . . . . .	57
6.2	Predicted and measured HPC efficiency recovery . . . . .	58
6.3	Predicted and measured HPT efficiency recovery . . . . .	59
6.4	Potential for efficiency recovery with operating time for HPC features . . . . .	61
6.5	Potential for efficiency recovery with operating time for HPT features . . . . .	62



# List of Tables

4.1	Exemplary matrix for component feature restoration due to workscoping	15
4.2	Hardware features relevant for turbo component performance loss . . .	17
5.1	Engine gas path parameters measured with serial instrumentation . . .	20
5.2	Observable component performance parameters . . . . .	22
5.3	Reynolds numbers and pressure loss coefficient for inlet, bypass and ducts	25
5.4	Analysis error induced by a HPC bleed mass flow change . . . . .	44
5.5	Standard variation of analysed performance due to nozzle exit area variation . . . . .	48
5.6	Types of simulated analysis uncertainties per underlying effect . . . . .	48
5.7	$\chi^2$ -homogeneity test for HPC and HPT efficiency . . . . .	50
5.8	$U_{95}$ (total uncertainty) for analysis using the booster capacity method .	52
6.1	LHS sample with 2 variables and 3 value ranges each . . . . .	56
6.2	HPC and HPT efficiency recovery comparison . . . . .	59
6.3	Optimised correlation factors for HPC workscoping . . . . .	60
6.4	Optimised correlation factors for HPT workscoping . . . . .	62
A.1	$U_{95}$ for analysed performance recovery due to measurement uncertainty	78
A.2	$U_{95}$ for analysed performance recovery due to FHV variation . . . . .	78
A.3	$U_{95}$ for analysed performance recovery due to nozzle exit area variation	79
A.4	$U_{95}$ for analysed performance recovery due to thrust reverser leakage . .	79
A.5	$U_{95}$ for analysed performance recovery due to booster capacity change .	79
A.6	$U_{95}$ for analysed performance recovery due to HPT capacity change . .	79
A.7	$U_{95}$ for analysed performance recovery due to measurement uncertainty	80
A.8	$U_{95}$ for analysed performance recovery due to FHV variation . . . . .	80
A.9	$U_{95}$ for analysed performance recovery due to booster capacity change .	80
A.10	$U_{95}$ for analysed performance recovery due to HPT capacity change . .	80



# Nomenclature

## Latin Letters

$A$	Area	$m^2$
$a, b, d$	Function coefficient	—
$B$	95% confidence estimate of the systematic uncertainty	—
$c$	Nozzle performance coefficient	—
$F$	Thrust	$N$
$f$	Scaling factor	—
$h$	Blade height	$m$
$k$	Linear factor	—
$M$	Mach number	—
$N$	Data Size, part count	—
$n$	Spool speed	$\frac{1}{min}$
$p$	Pressure	$\frac{kg}{m \cdot s^2}$
$Re$	Reynolds number	—
$S$	standard deviation of a sample population	—
$s$	Clearance	$m$
$T$	Temperature; Time (matrix)	$K; h$
$t$	Student-t factor; time	—; $h$
$U$	Uncertainty interval	—
$w$	Mass flow	$\frac{kg}{s}$

---

$X$	Hardware (feature) state	—
$Y$	Calculated/dependent parameter	—

**Greek Letters**

$\alpha$	Degree of restoration to performance exchange rate	%
$A$	Degree of restoration to performance exchange rate (matrix)	%
$\epsilon$	Error/Residual	—
$\eta$	Efficiency	—
$\Gamma$	Exponent for performance recovery potential (matrix)	—
$\gamma$	Exponent for performance recovery potential	—
$\lambda$	Ratio of systematic to random uncertainty	—
$\mu$	Mean value	—
$\Omega$	Independent function parameter	—
$\sigma$	Standard deviation	—
$\theta$	Sensitivity/ partial derivative	—
$\varphi$	Relative humidity	—
$\Xi$	Degree of feature restoration (matrix)	—
$\xi$	Degree of feature restoration	—
$\zeta$	Pressure loss coefficient	—

**Indices**

0	Starting time
0	Engine station: free flow
125	Engine station: fan exit
2	Engine station: fan inlet
25	Engine station: booster exit
3	Engine station: HPC exit
5	Engine station LPT exit

---

61	Engine station: exhaust nozzle core in the mixing plane
8	Engine station: nozzle exit
95	95% confidence level
<i>an</i>	Analysed parameter
<i>cl</i>	Clearance
<i>D</i>	Discharge
<i>enh</i>	Enhanced
<i>f</i>	Fuel
<i>H</i>	High speed spool
<i>j</i>	Running index for component groups
<i>j</i>	Running index for independent function parameter
<i>k</i>	Running index for features
<i>L</i>	Low speed spool
<i>l</i>	Left wing engine
<i>m</i>	Running index for restoration measure (repair, new part use)
<i>map</i>	Component map value
<i>max</i>	Maximum value
<i>meas</i>	Measured
<i>min</i>	Minimum value
<i>n</i>	Running index for clusters
<i>nom</i>	Nominal value
<i>p</i>	Running index for engines within a fleet
<i>post</i>	Post shop visit
<i>pre</i>	Pre shop visit
<i>pred</i>	Predicted
<i>r</i>	Right wing engine
<i>red</i>	Reduced parameter

---

<i>ref</i>	Reference
<i>s</i>	Static
<i>sys</i>	Systematic uncertainty (random part)
<i>tot</i>	Total
<i>tr</i>	Training data
<i>val</i>	Validation data

### Math Symbols

$\Re$	Measured parameter	—
-------	--------------------	---

### Abbreviations

<i>ACC</i>	Active Clearance Control
<i>BPR</i>	Bypass Ratio
<i>DOC</i>	Direct Operating Costs
<i>EEC</i>	Electronic Engine Controller
<i>EGT</i>	Exhaust Gas Temperature
<i>EMU</i>	Engine Monitoring Unit
<i>EPR</i>	Engine Pressure Ratio
<i>FADEC</i>	Full Authority Digital Engine Control
<i>FHV</i>	Fuel Heating Value
<i>GPA</i>	Gas Path Analysis
<i>HPC</i>	High Pressure Compressor
<i>HPT</i>	High Pressure Turbine
<i>LHS</i>	Latin Hypercube Sampling
<i>LOO</i>	Leave one out algorithm
<i>LPT</i>	Low Pressure Turbine
<i>MK</i>	Monitoring Kit
<i>MTBSV</i>	Mean Time Between Shop Visit



<i>OEM</i>	Original Equipment Manufacturer
<i>OV</i>	Outside Vendor
<i>SAS</i>	Secondary Air System
<i>SFC</i>	Specific Fuel Consumption
<i>TAT</i>	Turn-Around Time
<i>VSV</i>	Variable Stator Vanes
<i>WAR</i>	Water-to-Air-Ratio
<i>WPG</i>	Workscope Planning Guide



# Abstract

The increased importance of fuel consumption in the books of aircraft operators has led to a raised focus on the aspect of performance recovery for the engine overhaul process. It follows thus the need for a method to systematically and cost-efficiently investigate the impact of single workscope elements on engine efficiency.

A survey of existing studies and methods unearths recently developed methods for a comprehensive maintenance planning. These methods do not yet incorporate the aspect of performance recovery in spite of the high effort made to adapt engine specific workscope for observed hardware conditions. This is due to a lack of a systematic approach to establish a model correlating workscope and performance recovery. Research linking the two has so far been focused on predicting workscope-induced performance recovery based on pre-defined models and comparing the results with measured performance changes. No method for an adaptive model, based on available field data, has yet been established. Furthermore, any conceptual reflections to use field data to assess workscope impact on performance recovery are focused on the use of test cell data, rather than on-wing data recorded during engine operation.

To close this existing gap a new methodology is developed, correlating the engine overhaul's workscope and its effect. The workscope is therein defined by the degree of restoration which quantifies the percentage of parts for which a given feature is restored, either by repair or use of new parts. In order for the correlation model's extend to be manageable, the degree of restoration is defined for clusters comprising multiple stages.

The workscope effect, in terms of performance recovery, can be analysed using test cell or on-wing data both of which are subject to uncertainty induced by measurements and the engine model. It is demonstrated that the latter leads to lower analysis uncertainty for the high pressure components who are the primary lever for improvements on SFC and EGT-margin. This is explained by the improved accuracy achieved with averaging multiple snapshots. It is demonstrated that using an average of 50 filtered snapshots is a valid approach, since the engine components may be considered to be a system of

constant state during the operation time frame. Furthermore, the importance of the proper choice of the core flow analysis method is demonstrated, as well as the potential for analysis accuracy improvement using a more detailed engine model. It is shown that these measures have the potential of improving the analysis accuracy of HPC and HPT by a factor of 1.4 and 3.4 respectively. Analysis of recovered performance of fan and LPT is demonstrated to be more sensitive to installation effects. For these components, better accuracy can be achieved using test cell data, provided a performance test run is carried out prior to the overhaul.

In order to correlate workscope and performance recovery, a general functional relation is established to serve as the principal model. The model is then adapted to optimally fit available field data from past engine overhauls through implementation within an appropriate optimisation algorithm. An application to the high pressure components provides plausible results indicating clear distinctions between the leverage that different workscope elements provide for recovering performance. A cross validation using the leave one out algorithm shows the results of the correlation to be sensible. The potential for further improvement, for example by using measured dimension changes of the different features for the workscope description, is discussed. With this investigation, it is understood for the first time what the feasibilities and limitations in correlating workscope and performance recovery are. The established approach provides a basis for systems aimed at systematically planning engine worksopes with respect to performance restoration.

# Kurzfassung

Die gesteigerte Bedeutung von Kraftstoffverbrauch für die Wirtschaftlichkeit von Fluglinien hat zu einem erhöhten Fokus auf die Leistungswiederherstellung im Prozess der Triebwerkswartung geführt. Daraus leitet sich der Bedarf nach einer Methodik ab, mit deren Hilfe sich der Einfluss einzelner Wartungsinhalte auf die Triebwerkseffizienz systematisch und kosteneffizient untersuchen lässt.

Eine Recherche existierender Studien und Methoden zeigt kürzlich entwickelte Methoden für eine umfassende Wartungsplanung auf. Trotz der verstärkten Wartungspraxis, triebwerksspezifische Wartungsumfänge auf den Hardwarezustand anzupassen, beinhalten diese Methoden den Aspekt der Leistungswiederherstellung nicht. Es existiert kein systematischer Ansatz um Leistungswiederherstellung und Wartungsumfang zu korrelieren. Sämtliche Untersuchungen, die diese beiden Aspekte miteinander verbinden, basieren auf bestehenden Modellen für deren Zusammenhang. Diese Modelle dienen als Basis, um Leistungswiederherstellung auf Basis von Wartungsumfang zu prognostizieren und diese Prognosewerte anschließend mit gemessenen Werten abzugleichen. Es besteht aktuell keine Methodik zur Herleitung eines adaptiven Modells mit Hilfe von Felddaten. Konzeptionelle Überlegungen um Leistungswiederherstellung und Wartungsumfänge miteinander zu korrelieren basieren des Weiteren auf der Nutzung von Prüfstandsdaten anstelle von Daten, die im laufenden Flugbetrieb gesammelt werden.

Um die bestehende Lücke zu schließen, wird eine neue Methode entwickelt, die Wartungsumfänge von Triebwerken und deren Effekt hinsichtlich Leistungswiederherstellung miteinander korreliert. Der Wartungsumfang wird dabei mit Hilfe des Grads der Instandsetzung definiert. Dieser quantifiziert den Prozentanteil von Bauteilen, bei denen ein gegebenes, leistungsrelevantes Merkmal mit Hilfe von Reparaturmaßnahmen oder Neuteilverbau wiederhergestellt wird. Um die Detaillierung des Modells handhabbar zu machen, wird der Grad der Instandsetzung für Cluster definiert, welche mehrere Komponentenstufen beinhalten.

Der Wartungseffekt im Sinne von Leistungswiederherstellung kann mit Hilfe von Prüf-

standsdaten oder Daten aus dem laufenden Flugbetrieb analysiert werden. Es wird dargestellt, dass letzterer Ansatz zu einer höheren Analysegenauigkeit für die Hochdruckkomponenten führt, welche die primären Stellhebel für Wiederherstellung von SFC und EGT-Margin sind. Dies lässt sich erklären mit Hilfe der erhöhten Genauigkeit, die sich durch die Mittelung multipler Snapshots erreichen lässt. Es wird gezeigt, dass die Mittelung von 50 Snapshots einen validen Ansatz darstellt, da die Komponenten im betrachteten Betriebszeitraum als Systeme konstanten Zustands betrachtet werden können. Des Weiteren wird sowohl die Bedeutung der gewählten Analysemethode, als auch das Potential verbesserter Triebwerksmodelle für die Analysegenauigkeit, aufgezeigt. Es wird gezeigt, dass diese Maßnahmen das Potential haben, die Analysegenauigkeit um den Faktor 1.4 bzw. 3.4 zu verbessern. Es wird ferner aufgezeigt, dass die Analyse von Leistungswiederherstellung bei Bläser und Niederdruckturbine sensibler gegenüber Installationseffekten ist. Diese Komponenten können mit Hilfe von Prüfstandsdaten besser analysiert werden. Dies setzt jedoch einen zusätzlichen Prüfstandslauf vor dem Wartungsvorgang voraus.

Um Wartungsumfang und Leistungswiederherstellung zu korrelieren, wird eine allgemeingültige Funktion etabliert, welche das grundlegende Modell darstellt. Die Funktionskoeffizienten werden anschließend mit Hilfe von Optimierungsalgorithmen angepasst um die Felddaten vergangener Wartungsvorgänge fehlerminimal abzubilden. Die Anwendung dieses Ansatzes auf die Hochdruckkomponenten identifiziert die Primärhebel der Wartungsinhalte für die Leistungswiederherstellung eindeutig und plausibel. Eine Cross-Validierung unter Verwendung des „leave one out Algorithmus“ zeigt auf, dass die korrelierten Modelltrends sinnvoll sind. Die Potentiale für verbesserte Korrelationsmodelle werden diskutiert. Maßnahmen umfassen unter anderem die genaue Vermessung von Bauteilmaßen bzw. deren Veränderung im Rahmen der Wartung. Mit Hilfe der vorliegenden Untersuchungen wird zum ersten Mal verstanden, welches die Möglichkeiten und Beschränkungen bei der Korrelation von Wartungsumfängen und Leistungswiederherstellung bei Triebwerken sind. Die dargestellte Methodik stellt die Basis für Systeme zur systematischen Planung von Triebwerkswartung mit Hinsicht auf Leistungswiederherstellung dar.

# Chapter 1

## Introduction

In its 2011 study, Forbes magazine found that the number one concern in the global airline industry is the supply and cost of fuel, followed by regulations to curb carbon emissions [21]. The importance of fuel costs is underlined by the fact that they represent 20-25% of a typical airline's Direct Operating Costs (DOC) and up to 40% in the case of low cost carriers. Projections indicate an even further increase with fuel accounting for up to 50% of the DOC for a typical airline by the year 2020 [27]. Meanwhile, the industry is faced with an increase in competition and cost reduction pressure [76]. In order to operate profitably and maintain competitiveness, airlines are forced to reduce operating costs. Given the high share of fuel costs in DOC, airlines seek to realise parts of this reduction by demanding more fuel efficient aircraft. This demand impacts the development of both new airframes and new engines, with a major share of the improved fuel efficiency currently being due to better engine designs [3]. Requirements for lower fuel consumption also have an increased importance for the overhaul process with the focus being once again on the engine rather than the airframe. Manufacturers estimate that approximately two thirds of total aircraft efficiency loss is due to decreased engine efficiency [12]. This increases the focus on engines in aircraft overhaul. Engines are evaluated to be responsible for over 40% of an airline's total maintenance costs [19]. During operation, engine components are subjected to deterioration resulting in an increase of the engine's Specific Fuel Consumption (SFC) as illustrated in fig. 1.1. SFC increases due to performance losses of the components. Hence, the restoration of engine efficiency is now considered an overhaul requirement, alongside the restoration of mechanical integrity. This effect was first observed on a temporary basis during the oil crisis of the 1970's [59]. With oil costs projected to rise further in the mid-term and long-term outlook [51], the importance of fuel efficiency restoration will remain high.

For the overhaul process, SFC restoration is to be considered alongside other targets,

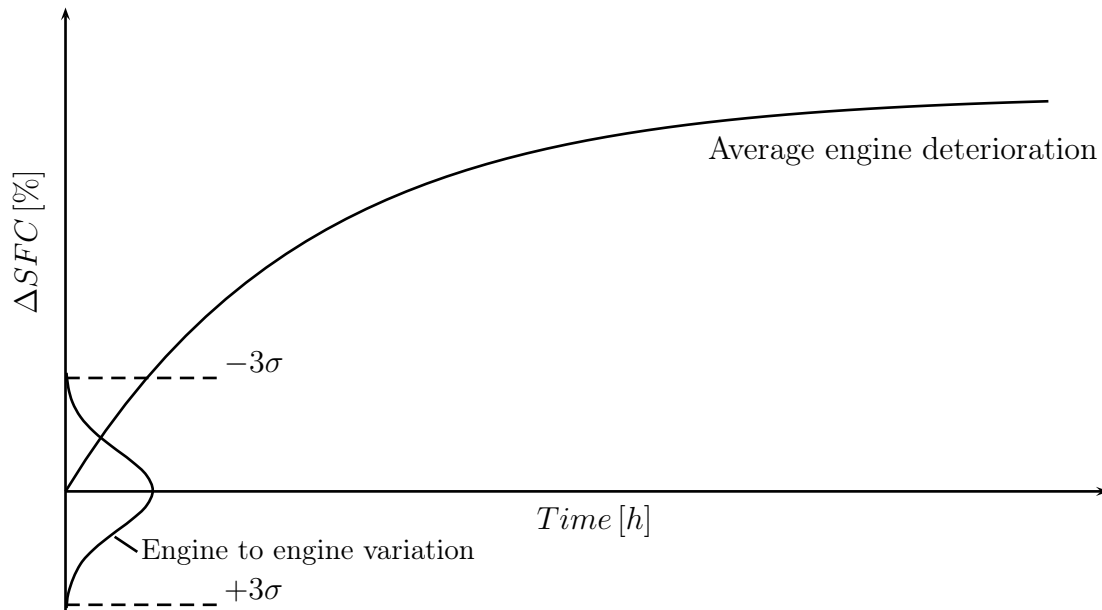


Figure 1.1: Generalized SFC deterioration as per [59], [66]

such as the restoration of engine life. For engine life, engine performance is attributed a key role, as low margins on Exhaust Gas Temperature (EGT), compressor surge line and spool speed have become relevant root causes for engine overhauls. This adds to the process complexity, which is furthermore increased by the fact that the hardware state of an engine is not known at the incoming stage. Hardware state may vary significantly between engines due to variations in the manufacturing process and operation [19], [62]. Hence, the challenge for the overhaul provider consists in defining an optimised overhaul for each individual engine.



## Chapter 2

# Existing Methods

Workflow management of any given manufacturing process is structured into four different aspects [67]:

- workflow content;
- workflow timing and duration;
- workflow space;
- workflow assignment.

Between these aspects, the workflow's content and timing are most prominently dependent on a system's hardware state. For repair processes, the issue of timing has been subjected in [30] and [73] with methods applicable to aero engines. In the case of the repair content, a division into further sub-aspects, defined by the principal overhaul targets, can be made. For an engine overhaul, the primary repair content are the repair instructions, presented to the engine shop. These repair instructions are named workscope. The workscope is defined, in coordination with the customer, based on the findings made during engine disassembly and inspection. The principle targets for a repair definition, aero engine or other machinery, are [70]:

- minimisation of Turn-Around-Time (TAT);
- minimisation of costs;
- maximisation of the repair quality.

The quality of the repair is defined by a system's post overhaul reliability and performance. The former aspect has been subjected in [30] by modelling the effects and benefits of a given workscope with respect to a reduction of failure probability during

continued operation. The present investigation fits into the latter aspect. It is aimed at correlating single workscope elements and their effect on engine performance.

The change in component and engine performance observed for repaired engines is due to feature changes of performance relevant hardware parts, such as a restoration of blade surface roughness [58]. There are multiple publications discussing impact modelling of one or few selected features for a specific component. An overview may be found in [65]. An aggregation of publications on the deterioration mechanisms causing the feature changes is given in [62]. A detailed discussion of the sources listed therein is waived for this work, so as not to go beyond its scope. Comprehensive works wherein relevant hardware features of performance relevant components are considered in an entirety are rare. In [65], such an approach is used while focusing on hardware and performance variation found in new production engines. In [62], a comprehensive approach is established in order to investigate engine deterioration due to operation. Probabilistic component performance during operation is modelled, using the model developed in [65], considering both performance variation due to production scatter, as well as due to differently deteriorating engines. A similar deterioration model is used in [48], with the focus set on predicting maintenance costs. This investigation considers both aspects of mechanical integrity and performance as the triggers for and cost drivers of an engine shop visit. All three works use an approach wherein the correlation between a component's hardware features and its performance is predefined. The impact on overall engine performance parameters is then predicted with performance calculations. For validation, the results are compared with test cell data and on-wing data respectively. Furthermore, they aim at predicting the time between maintenance events already during the design phase. Hence, their application in an operative environment seems to be limited.

In this context it is clear that existing studies leave open the subject of correlating workscope and performance changes. The principal idea has, however, already been discussed and non-comprehensive studies have been carried out. In [58], it is discussed to record maintenance and performance data for the purpose of correlating maintenance events with performance. The general idea, however, is dismissed due to the lack of efficient IT solutions. The lack of available data to assess performance changes for a given workscope is circumvented in [33]. It is proposed to simply trend engine and component performance parameters in order to detect shifts of the typical overhaul process within a fleet. In order to improve trend accuracy it is suggested to classify workscope and subsequently filter for similar overhauls. The study names the option to analyse on a modular level, in addition to solely observing overall engine parameters,

as a key element. In [15], it is suggested to use engine data, prior to and following the overhaul, coupled with workscope records, to deduce the performance effect of an overhaul. Global performance parameters, such as EGT, thrust and spool speed are investigated. Test data is compared with predicted values for different workscope. Reasonable agreements between predicted performance recovery and observed values is achieved. In [22], a different approach is used. The impact of single workscope on performance is investigated with multiple back-to-back engine test cell runs. Due to the costs of non-mandatory engine tests, the number of investigated workscope is limited.

The overview of existing methods shows that there is a lack of studies providing a comprehensive approach to relate workscope with component performance changes in an operational environment. This lack is due to:

- a lack of information on component performance state before the shop visit;
- limited instrumentation allowing for only few components to be observed;
- a large number of engine parts with impact on performance that is relevant when summed up but not singularly large enough to be observable.

The potential business benefit of being able to correlate workscope and performance impact is generally agreed to be immense. It would allow for an improvement of the input-to-output ratio of engine overhauls, as well as for a different quality of discussion between maintenance provider and aircraft operator.



## Chapter 3

# Project Objective and Proceeding

The aim of this research is to provide a means to correlate the workscope and the performance recovery of overhauled engines. In this context, it is important to understand what the natural limitations of such a correlation are. Following the framework established in chapter 1, the correlation's principle requirements are, that:

- it shall be applicable to different engine designs for the derivation of individual impact models;
- it shall be able to integrate any hardware feature with an impact on performance recovery due to overhaul;
- the correlated parameters shall be physically interpretable, thus providing transparency of the result;
- it shall be based on data which is easily accessible by independent maintenance providers.

In order to meet these requirements, as well as to overcome the obstacles discussed in chapter 2, the methodological investigation is build on three pillars as shown in figure 3.1. The *Assessment of the Overhaul Workscope*, shall quantify the hardware change induced by an engine overhaul. This entails the establishment of a parameter describing the workscope based on available hardware records not containing geometric measurements. A sensible degree of detail to which part groups have to be separated has to be established. The *Assessment of the Overhaul Effect* shall be based on available on-wing data. The accuracy limits of this assessment are to be established and compared to the accuracy of a potential performance recovery assessment with test cell data. Furthermore, the most accurate method of assessing performance recovery shall be determined. Finally, the *Correlation of Overhaul Workscope and Effect* links workscope

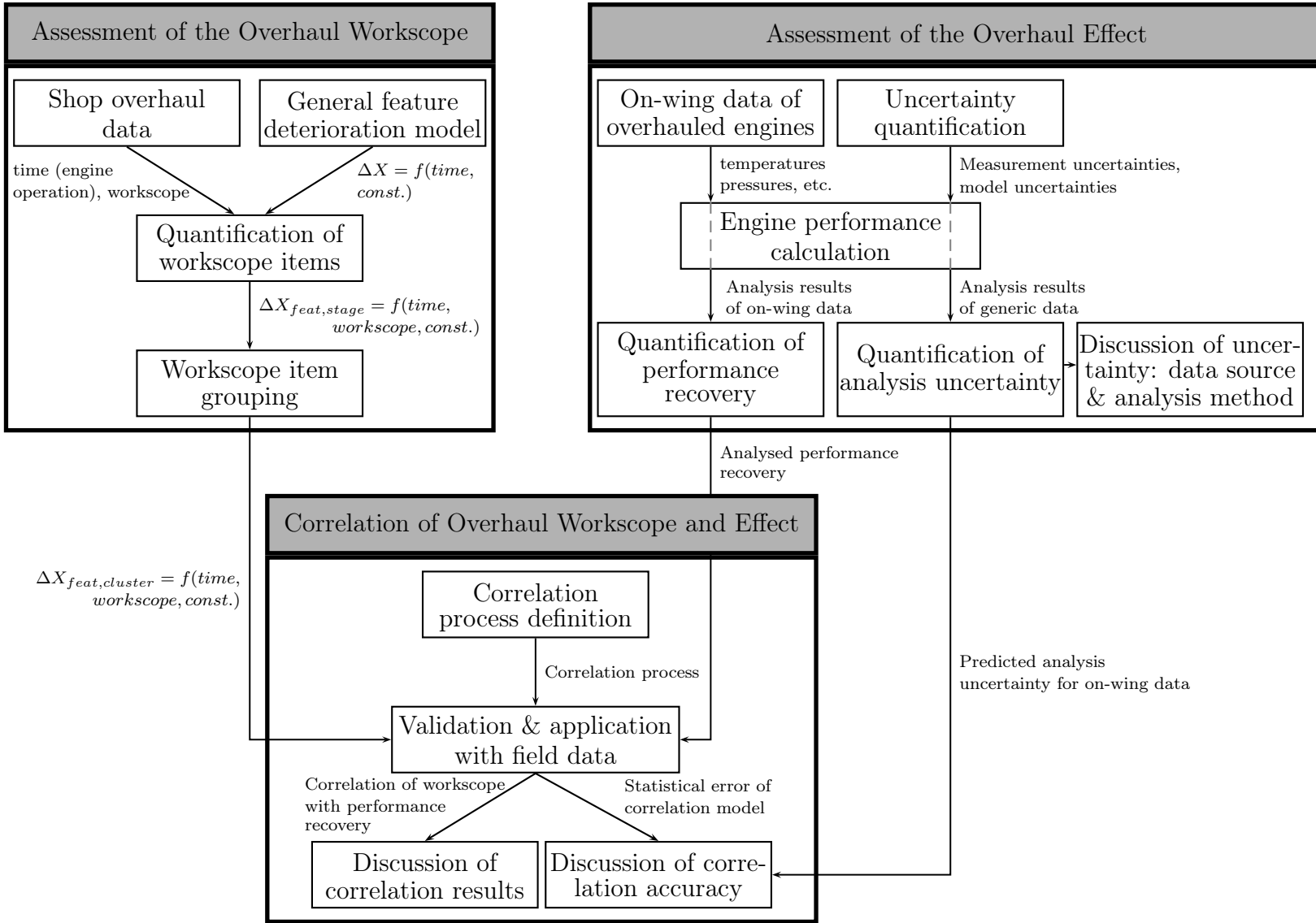


Figure 3.1: Scheme of the project architecture

and performance recovery. The correlation shall be validated with the available engine field data for workscope and for observed performance recovery. The uncertainty of the correlated model is to be compared to the predicted limitations of the performance recovery assessment. Furthermore, the resulting values of the correlation are to be discussed and physically interpreted.





## Chapter 4

# Assessment of the Overhaul Workscope

### 4.1 Operation-Induced Feature Changes

The general phenomenon of hardware changes during engine operation is referred to as deterioration. In order to define the potential for a feature's restoration during overhaul, it is necessary to understand its incoming state at the point of overhaul. This might be derived from its operational history [62]. A general functional statement describing the relation between a given technical system's operating time and the deterioration-induced change of the state  $X$  of a hardware feature  $k$ , is given in [17]:

$$\Delta X_k = a_k \cdot t^{1/b_k} \quad . \quad (4.1)$$

Therein the variable  $t$  is, depending on the underlying mechanisms, either measured in operating cycles or hours. The linear coefficient  $a_k$  indicates the deterioration extent. The deterioration rate is determined by the coefficient  $b_k$ , which depends on the deterioration type:

- $b_k < 1$ : exponentially progressing deterioration (observed for example for fretting);
- $b_k = 1$ : linearly progressing deterioration (observed for example for sliding abrasion);

- $b_k > 1$ : digressive deterioration evolution (observed for example for running-in processes).

The model as per equation 4.1 has already been applied to aero engines in [61], where the efficiency loss of turbo components over time is modelled with  $b = 2$ . In [58], the principal characteristic of the function is also applied to turbo component efficiency losses, which are, depending on the underlying mechanism, modelled to be of linear or digressive evolution. These models are validated with field hardware data. In [58] it is shown, that for some mechanisms deterioration is delayed at the start, resulting in a constant hardware state at the beginning of engine operation. Such a delay can be due to protective measures such as hardware coatings [13]. In order to incorporate this effect, equation 4.1 is modified by the parameter  $t_{0,k}$ , describing the time until which no deterioration of a feature occurs:

$$\Delta X_k = a_k \cdot \max(0, t - t_{0,k})^{1/b_k} \quad . \quad (4.2)$$

As per [58], the nature of turbo component deterioration mechanisms is modelled to be either linear or digressive. It is noted, that contrary to this model, burn-back of High Pressure Turbine (HPT) nozzles constitutes a mechanism which is of progressive nature [11]. However, this mechanism was not observed for the engine fleet used in this investigation. The boundary condition  $b_k \geq 1$  is thus imposed for this investigation. The deterioration model of equation 4.2 describes a typical feature evolution with operating time. For the present case, it represents the mean evolution for an engine fleet. The actual hardware state of a single engine may be described by a probabilistic model incorporating engine specific scatter about the mean evolution [65], [62]. This model, enhanced by the initial period of zero deviation, is illustrated in figure 4.1. Feature scatter is already observed for new engines due variations in the production and build processes [65]. Following the beginning of deterioration, the scatter increases due to engine-to-engine variations in the deterioration rate. These variations are explained by different environmental and operating conditions [62]. Furthermore, they can be caused by engine-specific deviations from mean duration of a flight cycle [65] or by on-wing maintenance actions [56]. A common probabilistic deterioration model may be used for a homogeneous fleet, with a similar variation of environmental and operating conditions for all engines. For the purpose of this investigation, a mathematical description of the mean deterioration is used. The probabilistic character of actual deterioration is, however, to be kept in mind and subject for discussion of the investigation's results later on.

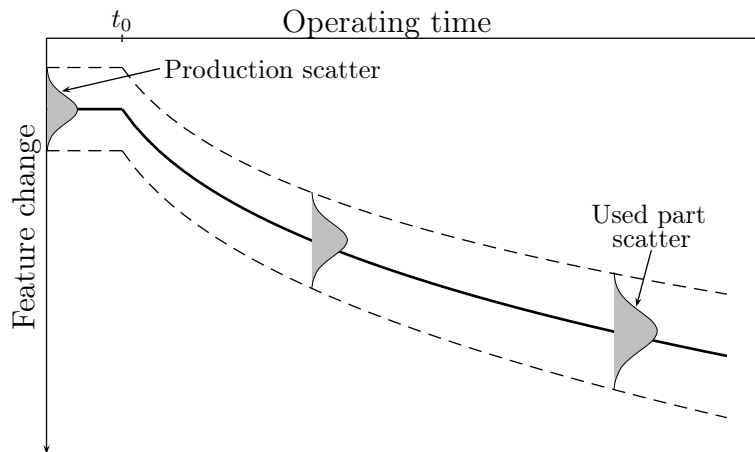


Figure 4.1: Schematic representation of probabilistic hardware feature evolution (on the basis of [65])

## 4.2 Modelling Overhaul-Induced Feature Restoration

Performance recovery can be realised during engine overhaul by restoring deteriorated features. In current practice, feature states prior to and following the engine overhaul are not persistently monitored. This is due to associated costs, as well as restraints on shop capacities and TAT. An alternate parameter describing feature restoration is therefore needed. This parameter is required to

- be based on input data recorded during the overhaul;
- be applicable to all performance relevant features;
- integrate different means used to restore a common feature.

The latter requirement refers to the restoration of a feature being realisable through part repairs or replacement with new parts. Repairs may be further sub-categorised. Standard repairs are made available in the engine maintenance manual. Their execution is licensed to maintenance providers and Outside Vendors (OV). Non-manual repairs may be developed by the maintenance provider and applied once clearance by the authorities has been granted.

Both manual repairs and non-manual repairs are aimed at restoring features to the hardware's new state. The two are therefore modelled to have the same mean effect on features as new part consumption. In practice, due the different processes of repair and new part consumption, the resulting mean effects will deviate from one another. Hence, an uncertainty of the chosen model results which is to be kept in mind and

subject for discussion of the investigation's results later on.

All three operations are modelled to reverse the process of feature deterioration from new production to the shop incoming state, quantified in equation 4.2. In order to account for the fact that not all hardware parts are overhauled, the degree of restoration is introduced as a workscope measure, analogously to the characteristic consumption factor presented in [17]. The degree of restoration  $\xi$  of the feature  $k$  of a component group  $j$  is described by the number of parts subjected to a restoration measure  $m$ , divided by the total number of parts of the component group. This relation is documented in equation 4.3:

$$\xi_{j,k} = \frac{N_{j,k,m}}{N_{j,tot}} \quad . \quad (4.3)$$

With equation 4.3 and the inverse of equation 4.2, the component group's mean feature restoration can be modelled. It is described by equation 4.4:

$$\Delta X_{j,k} = -a_{j,k} \cdot \xi_{j,k} \cdot \max(0, t - t_{0,j,k})^{1/b_{j,k}} \quad . \quad (4.4)$$

The degree of restoration can be derived from recorded overhaul data since every repair is designated one feature's restoration. The complete workscope therefore includes a mix of multiple repairs per part and allows for a separate tracking of the restoration for each feature. Workscoping information used for tracking is found in:

- the workscope planning records;
- material consumption tracking systems;
- route cards archived in engine build records;
- modification tracking systems.

Channeling all available information stored in these sources in order to calculate the feature restoration requires a thorough study of the overhaul process. Using the engine manual and certification documents of the internally developed repairs, an overview is established in matrix form, indicating all measures by which a feature can be restored. This is illustrated in table 4.1.

	Restoration of ...				
	stage 1		stage 2		...
	feature 1	feature 2	feature 1	feature 2	
Engine manual repair I	x				
Engine manual repair II			x		
Engine manual repair III	x		x		
Non-manual repair i	x		x		
New parts stage 1	x	x			
New parts stage 2			x	x	
...			x	x	

Table 4.1: Exemplary matrix for component feature restoration due to workscooping

### 4.3 Regard of the Level of Detail

The established model for overhaul-induced feature restoration can be used for correlation on a stage-wise basis. However, this is not practical as performance effects of singles stages are not observable with engine production instrumentation. Therefore, the level detail of the correlation needs to decreased.

Clustering provides a practical approach to the reduction of complexity based on similarity considerations [64]. In [65] and [50], for example, feature variation of the High Pressure Compressor (HPC) are considered on a whole component basis. In the present case, clustering based on similarity regarding the potential for performance recovery is expedient. This requirement can be further broken down into similarity of the impact on performance and similarity of feature changes. Hence, component groups which are of similar material and are subject to similar deterioration mechanisms, thus exhibiting similar feature changes, form a cluster if their impact of feature change on performance is similar. Assuming, for example, that the deterioration of the compressor front stages is dominated by erosion along the blade height and the deterioration of the compressor rear stages is mainly due to changes of the blade tip clearance, the compressor is separated into a front and a rear part.

For a selected cluster, the degrees of restoration can be calculated. For a cluster  $n$  of multiple compressor stages or turbine stages, the degree of restoration  $\xi_{n,k}$  of a feature  $k$  is herein defined as the arithmetic mean of all  $\xi_{j,k}$  of that cluster's stages:

$$\xi_{n,k} = \bar{\xi}_{j,k} \quad . \quad (4.5)$$

Equation 4.5 can mathematically be enhanced using weighing factors in order to assign an individual leverage to each stage. As the proposed cluster does already separate the higher loaded front stages from the rear ones, the use of weighing factors is waived. Analogously to equation 4.4, the cluster's feature restoration is defined as:

$$\Delta X_{n,k} = -a_{n,k} \cdot \xi_{n,k} \cdot \max(0, t - t_{0,n,k})^{1/b_{n,k}} \quad . \quad (4.6)$$

## 4.4 Identification of Performance-Relevant Features

The underlying mechanisms impacting deterioration, such as erosion or fouling, are well covered in open literature. The features impacted by these mechanisms are understood. A comprehensive overview may be found in [62]. The resulting list of features subject to deterioration and with an impact on performance is extensive. For a purposeful correlation, it is important to determine reasonably which features are expendable in the deterioration modelling process, thus permitting an extraction from the list of primary levers for performance restoration.

The potential for such a reduction in complexity is demonstrated in [65]. It is shown that the eleven most influential features, of the different engine components, explain more than 90% of the observed engine-to-engine scatter in SFC for new production engines. The 20 most influential features explain above 97% of the SFC scatter. A similar finding is made in [58] for deterioration-sensitive features impacting performance. Based on the findings presented therein, an overview of the relevant hardware features with an impact on component performance loss, is presented in table 4.2.

Rotor tip clearance is reported to be the most important feature, impacting both efficiency and capacity of all turbo components except for the HPT. For the HPT, the capacity is governed by the vane throat area. Medium efficiency losses due to increased surface roughness have been observed for all compressors, whereas typical roughness increases observed throughout operation cause only negligible turbine performance changes. Changes in airfoil contour induce performance deviations of the fan and the HPC. For the former, the reported contour change is a blunting of the blade leading edge, while the latter has been assigned to non-negligible changes of its blade leading and trailing edge angles, as well as thicknesses. HPT efficiency and capacity have been related to a twisting of the vane, which creates a leakage flow path at the inner platform. A last aspect highlighted in [58] is a change of turbine area, due to

	Fan		Booster		HPC		HPT		LPT <sup>1</sup>	
	$\eta$	$w_{red}$	$\eta$	$w_{red}$	$\eta$	$w_{red}$	$\eta$	$w_{red}$	$\eta$	$w_{red}$
Blade clearance (tip and/or liner loss)	++	++	++	++	++	++	++	0	++	++
Blade profile (angle change & thickness loss)	0	0	0	0	++	++	0	0	0	0
Blade leading edge contour (blunting)	++	++	0	0	0	0	0	0	0	0
Airfoil surface roughness	+	-	+	-	+	0	0	0	0	0
Vane twist (for inner platform form-fitting)	0	0	0	0	0	0	++	++	0	0
Vane trailing edge bowing	0	0	0	0	0	0	0	++	0	0

Table 4.2: Hardware features relevant for turbo component performance loss due to deterioration(++:high, +:medium, 0:none/negligible, -: not specified) as per [58]

bowing of the vane trailing edge, which impacts the HPT’s capacity only. The findings of [58] do not present any evidence as for any relevant potential for performance recovery due to HPC vane clearance restoration. It is noted, that this does not provide an indication for vane clearance not having any impact on HPC performance, but rather of it not being subject to an increase due to deterioration.

A principal sameness of feature-induced performance impacts between different engine types cannot be assumed [65]. Furthermore, differences in engine operation prohibit a generalization based on reference data. However, the presented findings may be used as a best possible approximation of feature-induced performance losses. The classification shown in table 4.2 is therefore used as the basis for this investigation’s correlation. Features with a medium or high relevancy for performance loss are considered for the correlation, while those with no or a negligible impact are disregarded. Turbine vane twist is not considered in this study, as the used engine design does not incorporate a form fitting construction of the HPT’s second vane inner platform, so as to prevent leakage flow over the stator cascade. Instead a seal construction between the stationary platform and the rotating disc is used to prevent leakage flow. Based on the findings presented in [77], seal clearance increase is thus considered as a source for HPT efficiency and capacity change.

---

<sup>1</sup>LPT: Low Pressure Turbine





## Chapter 5

# Assessment of the Overhaul Effect

With modern engines, a means to assess the performance state prior to and following the shop visit is available in the form of monitoring data recorded during operation. The share of engines, within the global fleet in operation, for which such on-wing data is recorded is substantial with a trend towards full coverage. Between 2004 and 2009 alone, their global share was estimated to rise from 50% to 70% [7]. Meanwhile, civil turbofan engines are increasingly well instrumented, as shown in figure 5.1.

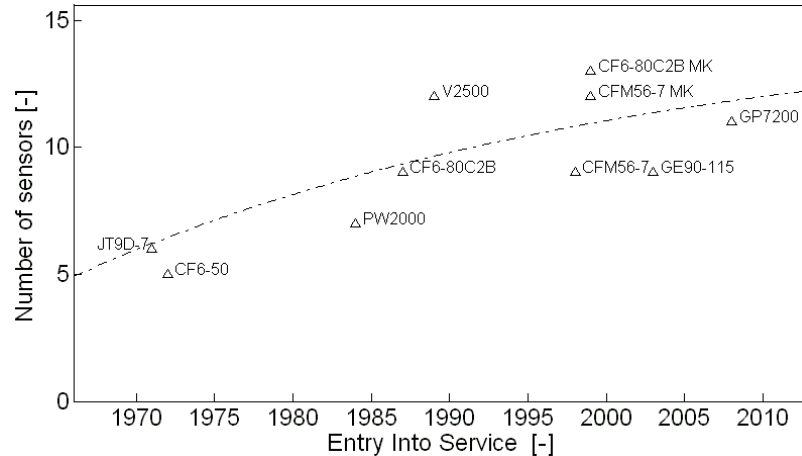


Figure 5.1: Evolution of monitored gas path measurements [38]

The number of sensors has increased beyond the scope of parameters, needed for the engine control system, allowing for a more detailed component analysis. Also, auxiliary parameters, such as bleed pressures or bleed mass flows, are observed to be included in the transmitted monitoring data of one or more recent engine designs. Sensors additional to the baseline are sometimes offered by Original Equipment Manufacturers (OEM) as Monitoring Kits (MK) to meet the increasing demand in health monitoring applications.

## 5.1 Demonstration of the Assessment Methodology

The methodology applied to the assessment of the effect of maintenance on engine performance shall be demonstrated using a realistic example. A two-spool turbofan engine with a high Bypass Ratio (BPR) and a mixed nozzle configuration is chosen. It is typical of an engine installed on a short- to medium-range, narrow-body, twin-jet, commercial passenger aircraft. The engine represents a 1990's technology and features a Full Authority Digital Engine Control unit (FADEC). The engine is equipped to measure 12 parameters that can be used for component analysis, listed in table 5.1. The flight Mach number is provided as an additional parameter by the aircraft instrumentation. Furthermore, ambient pressure and temperature are measured through the aircraft instrumentation. These parameters may be used as an alternative to the engine's inlet condition measurements, depending on which one provides the higher accuracy.

Sensor of ...	Name	Parameter
engine	$T_2$	Inlet temperature
	$p_2$	Inlet pressure
	$p_{125}$	Fan exit pressure
	$T_{25}$	Booster exit temperature
	$p_{25}$	Booster exit pressure
	$T_3$	HPC exit temperature
	$p_{s3}$	HPC exit static pressure
	$EGT$	Exhaust Gas Temperature (LPT exit)
	$p_5$	LPT exit pressure
	$n_L$	Low pressure spool speed
	$n_H$	High pressure spool speed
	$w_f$	Fuel mass flow
aircraft	$T_0$	Free flow temperature
	$p_0$	Free flow pressure
	$M$	Mach number

Table 5.1: Engine gas path parameters measured with serial instrumentation

Field data is taken from one operator. The served network's environmental conditions are as typically found for a European or Northern American operator. An analysis of the fleet's rotation shows for all aircraft to be equally dispatched within the route network. The probability distributions of environmental factors impacting engine hardware, such as particle type and concentration of the air, can thus be assumed to be equal for all aircraft [62].

Aircraft altitude, flight Mach number, temperature deviation from standard day con-

ditions and the power rating Engine Pressure Ratio (EPR) are analysed to vary with a normal distribution between flights. A fleet analysis shows engine power settings, flight Mach number and ambient conditions to be of equal probability distributions for all aircraft.

With the monitoring data collected during cruise operation, component states are analysed using Gas Path Analysis (GPA), a standard performance calculation method. It is also validated for scenarios of only single stages of an analysed component being subject to a change in performance [47]. Performance calculation generally constitutes a discipline that is well-established and discussed in open literature, such as [49] and [72]. Therefore, a detailed discussion is waived at this point.

Total engine mass flow is assessed using the capacity curve of the mixed nozzle. Measurement of the core mass flow is not available in engine production instrumentation and needs to be analysed using either of the following approaches [31]:

- analysis based on the known capacity of one of the core's turbo components;
- analysis through a heat balance equation for a control volume of known fuel mass flow, as well as known inlet and outlet temperatures.

Each core flow analysis method poses particular constraints with regard to the problem of performance recovery analysis. For example, using a component's capacity characteristic for core flow analysis is most sensible if its capacity is not changed during the engine shop visit due to that component not having been overhauled. When analysing performance recovery this is to be considered, as well as the fact that each component's analysis uncertainty varies between the applied core flow analysis methods. In other words, for a given component some analysis methods yield more precise analysis results than others. In the case of the heat balance method, the fact that it requires a turbine temperature measurement is problematic for performance recovery analysis. Temperature profiles in the hot section are inhomogeneous and depend on combustor characteristics such as variation in fuel nozzle capacities or cooling flow field in the liner vicinity [22]. These characteristics often do change throughout the overhaul process due to fuel nozzle cleaning or a change of their circumferential position. Overhaul records furthermore showed EGT sensors to be often replaced during overhaul due to faulty functioning prior to the shop visit. EGT measurements are thus disregarded in this investigation and only the core flow analysis methods using capacity characteristics are considered in the following.

### 5.1.1 Modelling of Non-Observable Turbo Components

In order to improve the results of the analysed performance recovery, the engine performance model has been enhanced with respect to non-analysed parameters and secondary performance effects. In table 5.2 an overview is given which parameters can be analysed directly based on the available instrumentation.

Core flow analysis method	Fan		Booster		HPC		HPT		LPT	
	$\eta$	$w_{red}$	$\eta$	$w_{red}$	$\eta$	$w_{red}$	$\eta$	$w_{red}$	$\eta$	$w_{red}$
Booster capacity	-	x	x	-	x	x	x	x	x	-
HPT capacity	-	x	x	x	x	x	x	-	x	-
LPT capacity	-	x	x	x	x	x	x	x	-	-

Table 5.2: Observable component performance parameters for different core flow analysis methods

Fan efficiency cannot be analysed directly. In [58], it is proposed to couple fan efficiency loss and fan capacity loss. As shown in table 4.2, fan deterioration is primarily due to two degradation mechanisms, which inversely are also the mechanisms for potential performance restoration. It is primarily caused by deterioration of the rotor leading edge and an increase in tip clearance. Test data for engine-specific impact of leading edge deterioration and tip clearance increase on fan performance is not available. Therefore, experiences from a reference engine is used as suggested in [45]. The effects of a changed leading edge geometry for transonic fan blades have been studied in [23] and [74] for a CFM56-5 engine. The decrease in fan efficiency was found to be 1.75 times higher than that of fan capacity. For the fan tip clearance a ratio of 1.15 was found [63] for the same engine. For an overhaul including a restoration of the main features, the ratio of recovered efficiency to recovered capacity is expected to be between those values. The fan efficiency scaling factor is therefore modelled, using the arithmetic mean, to have a degradation 1.45 times as high as the fan capacity scaling factor:

$$f_{\eta} = 1 + 1.45 \cdot (f_{w_{red}} - 1) \quad . \quad (5.1)$$

The used ratio of 1.45 compares well to the findings presented in [61], where the ratio of total fan efficiency loss to total fan capacity loss due to deterioration is analysed to be 1.6 based on field data of a JT9D engine.

LPT capacity is used to separate the efficiencies of the two turbine components. For

engines subject to an LPT overhaul, which are however uncommon, this induces an error in the analysis of recovered turbine efficiencies. Changes in LPT capacity with operation are due to changes of the tip clearance, as are changes of its efficiency as discussed in [58]. Therein, the ratio of efficiency change to capacity change is analysed to be  $-1.5$ . Further studies, quantifying the ratio of clearance-induced capacity change and efficiency change of LPTs, are not available. The LPT capacity scaling factor is therefore modelled to have an increase 0.67 times as high as the LPT efficiency loss.

$$f_{w_{red}} = 1 - \frac{f_{\eta} - 1}{1.5} \quad . \quad (5.2)$$

The correlation can be applied when using booster or HPT capacity for core flow analysis. Using the LPT capacity method, the LPT efficiency is not analysed and the correlation may not be applied. This core flow analysis method should therefore only be applied for overhauls during which the engine's LPT is not overhauled. These engines are modelled to have an overhaul-induced LPT capacity change equal to zero. As mentioned above, overhaul data available to the author showed this to be a common case.

Changes of the booster capacity or HPT capacity need to be modelled when using the respective core flow analysis methods. A possible approach is to establish a theoretical model linking hardware data and capacity change [10]. An alternative approach is the use of model distributions [24], provided the changes in capacity can be considered to be the result of a random experiment. A random experiment is defined as an operation which is repeated under identical conditions [8]. In the present investigation, a fleet of engines is used which:

- are all of the same type. Differences of new engine performance can thus be explained by the probabilistic character of the processes of production and assembly [65];
- are all operated by one airline and with an identical route mix, which leads to equal probability distributions for environmental conditions and geographic locations. Performance loss, due to continuous operation or single events, may therefore also be described by a common probabilistic model [65];
- are all subject to the same overhaul processes for disassembly, inspection, repair and assembly. Workslope definition is based on identical requirements, defined in the engine manual and the Workslope Planning Guide, and the probabilistic incoming state of the engine hardware.

It is therefore assumed that changes of booster and HPT capacities are of random nature and may be described by a probabilistic model. The principal use of the probabilistic model is shown in figure 5.2 based on the HPT capacity method. Engines for which the HPT is not overhauled, are modelled to have an overhaul-induced HPT capacity change equal to zero. It is noted, that the HPT is also not disassembled for these engines. A build-rebuild-effect, discussed in [42], is therefore assumed to not occur. Engines for which the HPT is overhauled, are modelled to have a non-zero change in HPT capacity. The engine data base has been searched for overhauls where the LPT is not overhauled while the HPT is overhauled. Using the LPT capacity method for core flow analysis, a statistical variation of the change in HPT capacity has been established. The analysed statistical mean value is used to model changes of the HPT capacity. The statistical model is subject to errors. These errors and their impact on component analysis are subject to quantification in chapter 5.3.

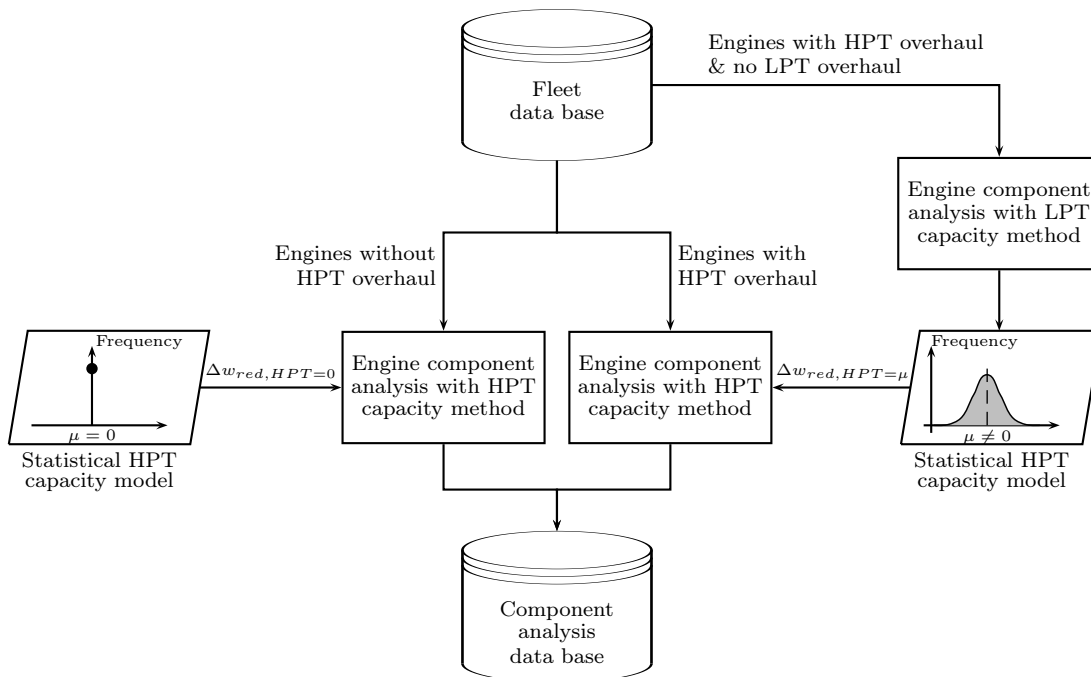


Figure 5.2: Setup of the statistical model for HPT capacity recovery

### 5.1.2 Modelling of Secondary Effects

In [39], it is shown that lack of a Reynolds number model for turbo component induces non-negligible uncertainties in the performance recovery analysis. Therefore, Reynolds number models have been set up for the fan, booster, HPC and LPT. For the HPT no

model is set up, given that its performance can be assumed independent of Reynolds number variations within cruise flight regimes [9].

For the combustion chamber no Reynolds number model is set up, as both its performance parameters, efficiency  $\eta$  and pressure loss  $\Delta p$ , can be considered independent of a change in Reynolds number [31].

Inlet, bypass, ducts and Turbine Exhaust Case are also not modelled to be subject to a performance variation due to alternating engine inlet conditions. The results of a preliminary analysis of the variations of their pressure loss coefficient  $\zeta$  are shown in table 5.3. The calculation is based on the approach presented in [69]. It is observed that the maximum deviation of the pressure loss coefficient, which is herein defined by the  $3\sigma$  variation of the operating conditions, is 4.1% for the Turbine Exhaust Case. Given a maximum design pressure loss of 1.5% for this component, as stated in [72] and [25], this translates in a standard deviation for the pressure loss of 0.02%. It is concluded that no Reynolds number effect modelling needs to be integrated in the models of inlet, bypass and ducts due to the low order of magnitude of uncertainty on component performance analysis.

	$Re_{nom}$ [-]	$Re_{nom} - Re_{min}$ [-]	$\zeta_{nom}$ [-]	$\zeta_{max} - \zeta_{nom}$ [%]
Inlet	$7.43 \cdot 10^6$	$5.18 \cdot 10^6$	0.0097	0.73
Bypass	$8.14 \cdot 10^6$	$2.26 \cdot 10^6$	0.0104	1.69
Swan Neck Duct	$1.90 \cdot 10^6$	$6.10 \cdot 10^5$	0.0134	2.33
Inter Turbine Duct	$1.20 \cdot 10^6$	$3.77 \cdot 10^5$	0.0143	2.59
Turbine Exhaust Case	$1.47 \cdot 10^6$	$4.63 \cdot 10^5$	0.0126	4.12

Table 5.3: Reynolds numbers and pressure loss coefficient: Nominal values and maximum deviations for inlet, bypass and ducts at cruise conditions

Simplifications of the performance model of the engine nozzle are also examined. The potential impact of a non-modelling of Reynolds number effects on analysis uncertainty of turbo components is contemplated. Considering the complex nature of the mixing process for core and bypass stream, the models proposed in [69] cannot be applied for the mixed exhaust nozzle. In [35], a method is proposed to include Reynolds number impact on nozzle performance in the engine model. Based on the Reynolds number of the core section in the mixing plane,  $Re_{61}$ , the variation of the nozzle discharge coefficient  $c_D$  is calculated as

$$\Delta c_D = 104.548 \cdot (Re_{61,ref}^{-1} - Re_{61}^{-1}) + 3.428 \cdot 10^7 \cdot (Re_{61,ref}^{-2} - Re_{61}^{-2}) \quad . \quad (5.3)$$

with  $Re_{61,ref}$  as the core Reynolds number in the mixing plane at map reference conditions.

The implications of a Reynolds number variation in the nozzle are visualized in figure 5.3. The regimes for which an impact on the discharge coefficient needs to be taken into account are shown in this image. In the Reynolds number regime of  $Re_{61,ref} = 4 \cdot 10^5$ , for example, a Reynolds number variation of  $-1 \cdot 10^5$  results in a variation of the discharge coefficients of  $-0.00025$ . It may therefore be considered negligible with respects to nozzle characteristics. For regimes of  $Re = 2 \cdot 10^5$  and below, the impact on the discharge coefficient does become non-negligible. This regime is typical of business jet flights, which operate at higher altitudes, but is usually not reached under cruise conditions of commercial airline operation. For this investigation's fleet, the Reynolds number of the nozzle core section in the mixing plane at mean cruise conditions is  $8.8 \cdot 10^5$ . Its  $3\sigma$  variation due to varying operating conditions is calculated to be  $\pm 1.94 \cdot 10^5$ . For a negative deviation this corresponds to a variation of the discharge coefficient of  $-0.00005$ . It is concluded that Reynolds number effects in the nozzle are of a negligible order of magnitude, as are the implications of a non-modelling on analysis uncertainty of other engine components. A Reynolds number model for the nozzle is thus not integrated in the engine model.

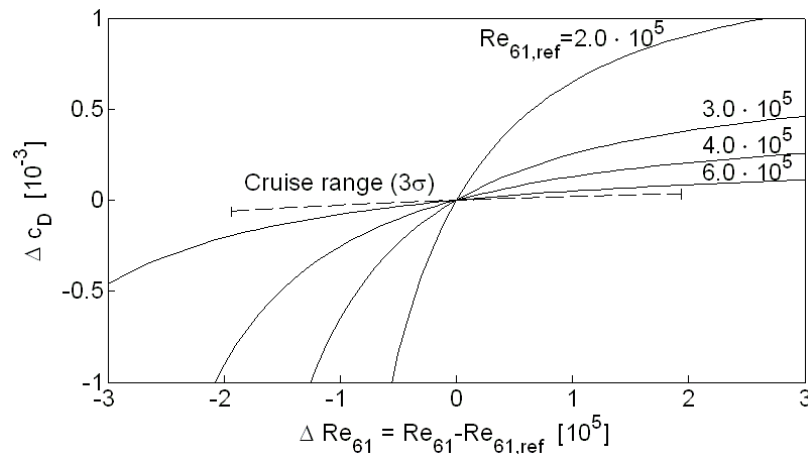


Figure 5.3: Nozzle discharge coefficient change due to Reynolds number variation

Variations of the operating conditions impact component characteristics also through a change of the tip clearance. An effect can be observed both on a turbo component's efficiency, as well as its capacity [36]. Changes of the tip clearance can be divided into transitory effects and steady state effects [20]. The former effects are disregarded in this



investigation, as cruise data is taken at stabilized operating conditions. Steady state variation of the tip clearance can be due to component load level, such as a variation of aerodynamic speed at constant inlet conditions, or a variation of the component inlet conditions at a given aerodynamic speed [31]. For the former, the variation can be integrated in the turbo component map [20], as is the case in the present model. Component maps are set up to represent performance at standard cruise conditions. For the latter, a correction model for the turbo components needs to be established. It is noted that, based on the findings of [20], the assumption is made that steady state clearance changes in the Secondary Air System (SAS) occur primarily in the regimes of part power operation. Their changes are therefore not modelled.

The principal physical effects of turbo components' steady state tip clearance changes due to varying inlet conditions at constant aerodynamic speed are [31]:

- thermally induced change of casing radius and thickness;
- mechanically induced changes of the casing radius through a variation of the inner to outer pressure difference;
- thermally induced change of disc radius and blade height;
- disc and blade radius change due to mechanical speed variation.

As suggested in [37], the change of mechanical speed is assumed to be the major contributor to the clearance change. Clearance changes induced by centrifugal forces are a function of actual mechanical speed and map speed [31]:

$$\Delta s = \text{const.} \cdot (n^2 - n_{map}^2) \quad . \quad (5.4)$$

The constant term in equation 5.4 is component specific and depends on rotor geometries and material properties. Correlation between clearance and performance changes have been subjected by numerous studies. The suggested models are both non-linear, e.g. [20] and [6], and linear, e.g. [50] and [45]. For the present investigation, a linear correlation is used. With equation 5.4, the dependency between relative speed change and the efficiency scaling factor is modelled as:

$$\begin{aligned} f_{\eta,cl} &= k_{cl} \cdot \Delta s / h \\ &= k_{cl} \cdot \text{const.} \cdot (n^2 - n_{map}^2) \quad . \end{aligned} \quad (5.5)$$

The capacity scaling factor is defined analogously. Given the small speed deviations between cruise data points induced by a variation of the inlet conditions, the linear model is further simplified:

$$f_{\eta,cl} \approx k'_{cl} \cdot (n - n_{map}) \quad . \quad (5.6)$$

The constant  $k'_{cl}$  of equation 5.6 is component specific. It incorporates component geometries, material properties and the exchange rate of clearance versus efficiency. Its value is a priori unknown to anyone but the OEM. However, using on-wing data it can be reverse engineered as shown in figure 5.4. HPC efficiency is analysed for a data set of 400 snapshots. A trend between the variation of the mechanical speed and the analysed efficiency scaler is observed, with a high scatter about the trend. With the given data a linear model has been established using a regression based on a least-square best fit. Due to the high scatter of the analysed scalars about the linear regression, the significance of the model is tested. The scatter about the regression line is explained by the analysis uncertainty of the HPC efficiency, which is relatively high compared to the latter's sensitivity to speed change. This is reflected by the regression's low  $R^2$  value of 0.37. However, the regression slope, which is tantamount to  $k'_{cl}$ , has a t-statistic of 15.36 and a p-value of  $4.35 \cdot 10^{-42}$ . The result can therefore be accepted with a significance level above 95% [53]. The high significance of the regression, in spite of the low  $R^2$  value, is explained by the large sample size. Analysis of data for other components did not indicate any noticeable clearance effects. A clearance model is thus setup for the HPC as the sole component.

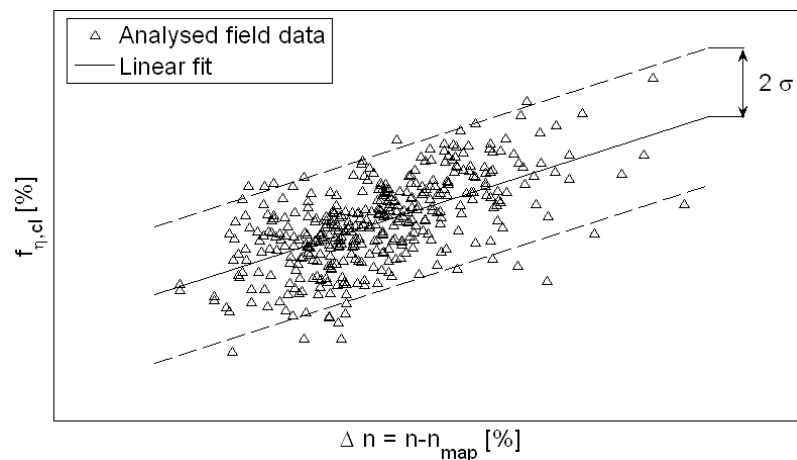


Figure 5.4: Linear clearance model for HPC efficiency based on field data

## 5.2 Measurement Uncertainties

### 5.2.1 Description of On-Wing Measurement Process

The typical measurement chain of an engine pressure measured on-wing is shown in figure 5.5. In the case of multiple pickups, pressures are averaged pneumatically. A pressure sense line routes the pressure to a transducer located within the Electronic Engine Controller (EEC). The electric current output signal of the transducer is processed into a digital signal by an analogue-to-digital converter. The information is sent electronically to the Engine Monitoring Unit (EMU) where it is stored temporarily. It is then processed for data reduction purposes and sent to a ground station from where it is transferred to a data storage server. In this measurement chain, all elements within the engine or aircraft are of unknown uncertainty for all parties but the OEMs. Uncertainty due to hardware or data processing within the EEC in particular, is strictly proprietary. Hence, a method is needed to assess uncertainty of the total measurement chain relevant for performance recovery analysis.

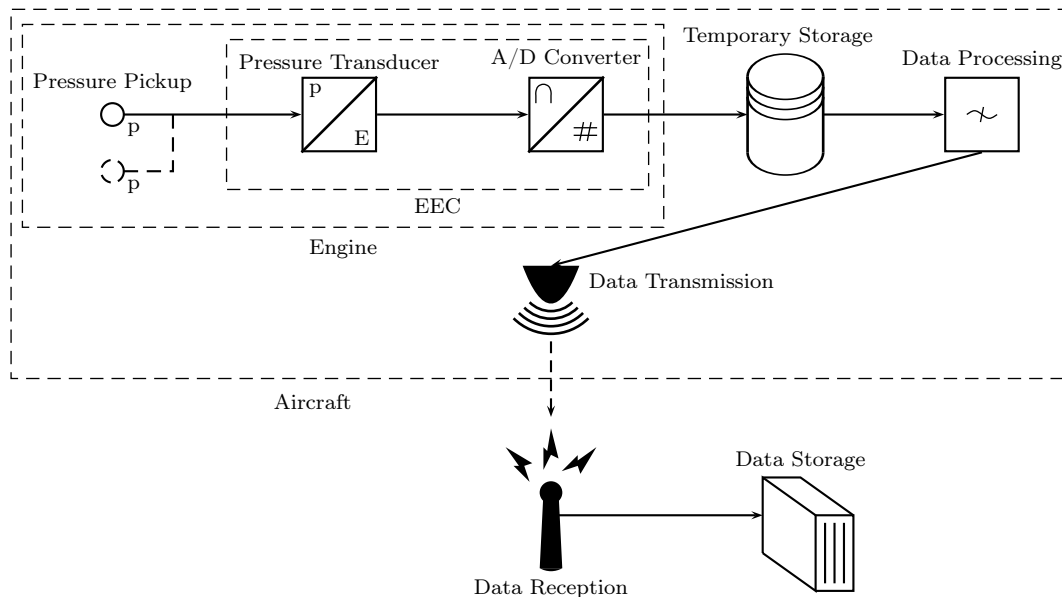


Figure 5.5: Pressure measurement chain of production pressure instrumentation

A measurement's error is divided into its systematic and its random error portions. In [5], the random error is defined as 'the portion of the total measurement error that varies in repeated measurements of the true value'. As furthermore stated, it can be attributed to non-repeatability in the measurement system, environmental conditions, data reduction techniques and measurement methods. Random measurement

uncertainty is quantified by its standard deviation  $\sigma$ . A sample population's standard deviation  $S$  is considered an estimate of  $\sigma$ .

Systematic error is constant for a parameter when repeatedly measuring a constant true value with a given installation. Its magnitude changes, however, between measurement installations [5]. Systematic error may be reduced through system calibration. Contributions to the systematic error left after calibration are referred to as the remaining systematic uncertainty which is considered to be of normal distribution [26]. The remaining total systematic uncertainty is commonly quantified by its 95% confidence estimate  $B$ . The stochastic part of the remaining systematic uncertainty may be assessed using inter-laboratory or inter-facility tests with a constant reference system being measured. The uncertainty's standard deviation is estimated with the statistical distribution of each facility's mean measurement [5]. In analogy to random uncertainty  $\sigma_{sys}$  and  $S_{sys}$  are used in the following to describe the actual and the estimated distribution of the stochastic part of the remaining systematic error.

For the assessment of performance recovery due to engine maintenance, random measurement uncertainty of all measured parameters needs to be considered. The remaining systematic uncertainty is neglected for all measurements where the error remains constant with the maintenance process. The resulting error in analysed performance is considered to be constant and thus canceled in a pre-to-post-maintenance comparison. The assumption of a constant remaining systematic error can be made for all measurements of the engine powerplant, as long as the measurement system remains unchanged. Any engines for which the corresponding measurement hardware was exchanged or re-calibrated during maintenance, are not used for this investigation. An exception to this is measurement hardware of the EGT. As discussed in section 5.1, EGT measurements are disregarded for recovery analysis.

For measurements of the engine's free flow respectively inlet conditions and the Mach number, the error induced by the remaining systematic measurement uncertainty is not constant. Their corresponding sensors are part of the aircraft fuselage respectively the engine cowling. Given that the overhauled engine is typically installed on a different aircraft following the shop visit than the aircraft it is dismantled from before the shop visit, the error varies due to the stochastic part of the systematic uncertainty. Distributions of the systematic uncertainty need thus to be taken into account for these measurements in order to assess the accuracy of the performance recovery analysis.

## 5.2.2 Field Data-Based Assessment of Random Measurement Uncertainty

For the assessment of the random measurement uncertainty, on-wing data of engines installed on the same aircraft is used. The on-wing data is assembled of data pairs, with each pair consisting of two cruise snapshots taken simultaneously for left wing and right wing engine. The engine ambient conditions and power setting are thus identical.

For each measured engine parameter  $\mathfrak{R}$  a deviation between both measurements is calculated. Depending on the parameter, the deviation is calculated as an absolute difference:

$$\Delta\mathfrak{R} = \mathfrak{R}_l - \mathfrak{R}_r \quad , \quad (5.7)$$

respectively as a relative one

$$\Delta\mathfrak{R} = \frac{\mathfrak{R}_l - \mathfrak{R}_r}{\mathfrak{R}_r} \cdot 100 \quad . \quad (5.8)$$

A comparison of a time series of data pairs yields a non-constant curve with a data scatter. For the series, a time frame is considered during which the engine on both wings remain installed and without a switch. An example for an aircraft's engine data is shown in figure 5.6.

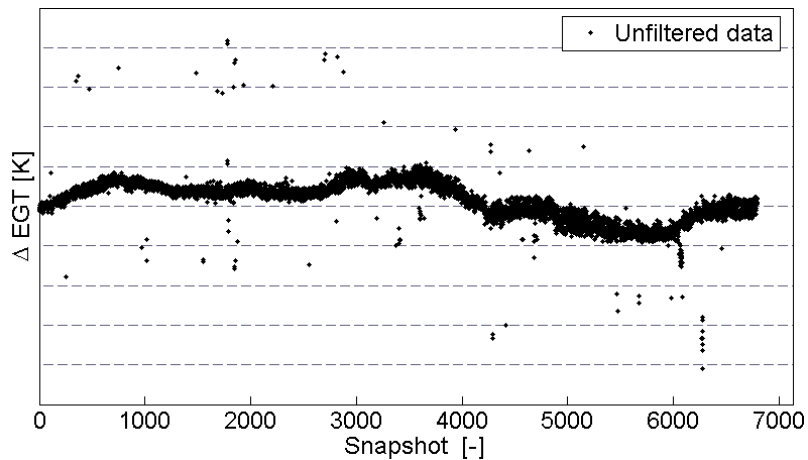


Figure 5.6: Deviation of left wing and right wing EGT before filtering

Deviations between the two measurements are due to a variety of underlying causes:

- stochastic part of the remaining systematic measurement error;
- random measurement error;
- different initial engine hardware states due to production scatter and past operation;
- different engine deterioration rates during the considered time frame;
- different power setting trims of the engines;
- different engine settings: Variable Stator Vanes (VSV) angle, engine bleeds, generator load or Active Clearance Control (ACC);
- measurement malfunction.

In order to obtain an estimate of the random measurement uncertainty, the raw data is processed via a series of filtering steps designed and discussed in [38]. The aim of the filtering process is to obtain a data set, whose scatter is primarily due to random measurement uncertainty of the measured parameters. In figure 5.7 the filtered data is shown. It is observed that scatter is decreased. In the course of the filtering process, scatter due to different engine settings is eliminated, as are outliers due to measurement malfunctions. Due to the former the complete time frame of the first 300 data points is also filtered out. Scatter due to different engine hardware states and engine trims is rendered negligible by filtering for data points with similar engine operating conditions.

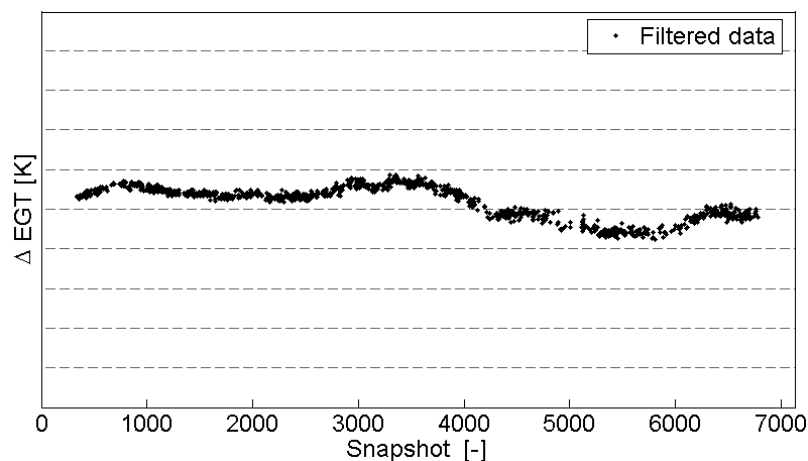


Figure 5.7: Deviation of left wing and right wing EGT after filtering

From the filtered data, constant offsets between left and right wing EGT and time-

dependent trends remain to be eliminated. Constant offsets are due to different initial engine hardware states, engine trims and the remaining systematic measurement error. The time-dependent trend observable in figure 5.7 is due to different engine deterioration rates during the considered time frame. For the purpose of their elimination, a centered smooth curve for the filtered data is established and the scatter about that curve is calculated. The used algorithm uses a range of  $\pm 25$  snapshots for the centered smooth curve. The remaining scatter, shown in figure 5.8, is primarily due to random

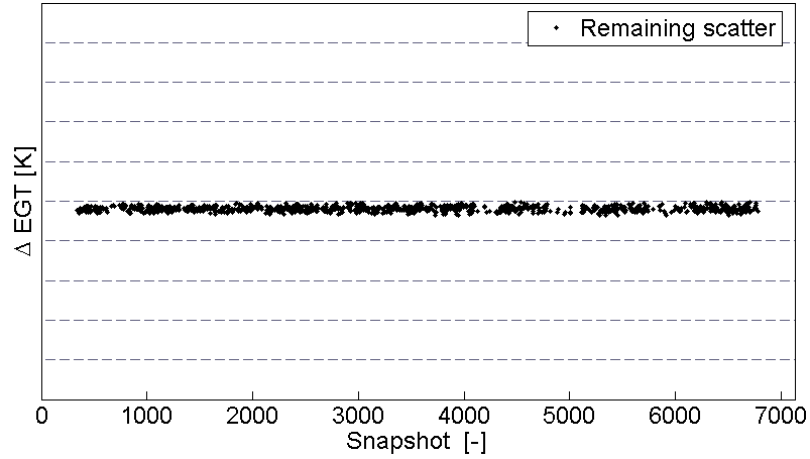


Figure 5.8: Smooth curve deviation of left wing and right wing EGT after filtering

measurement uncertainty. The processed data includes secondary effects. The standard deviation of the data shown in figure 5.8 is thus considered a conservative estimate of the random uncertainty of the engine measurements:

$$\sigma_{\Delta R} \leq S_{\Delta R} \quad . \quad (5.9)$$

From the random measurement uncertainty of the difference between left and right wing engine, the random measurement uncertainty of a measurement sensor can be deduced. The law of error propagation states that the standard deviation for a calculated parameter  $Y$  is a result of the standard deviations of the independent parameters  $\Omega_i$ , of which  $Y$  is a function [5]:

$$\sigma_Y = \sqrt{\sum_i (\theta_i \cdot \sigma_{\Omega_i})^2} \quad , \quad (5.10)$$

wherein the sensitivity  $\theta$  is given by the partial derivatives of dependent and indepen-

dent parameters:

$$\theta_i = \frac{\partial Y}{\partial \Omega_i} \quad . \quad (5.11)$$

It is assumed that both left wing and right wing engine have the same measurement hardware and thus the same random measurement uncertainty. With equations 5.9 and 5.10, the conservative estimate of the random uncertainty for a single sensor is thus deduced as:

$$\sigma_{\mathfrak{R}} \approx \frac{1}{\sqrt{2}} \cdot S_{\Delta \mathfrak{R}} \quad . \quad (5.12)$$

This approach results in the uncertainty of all engine measurements shown in table 5.1. For a representative assessment of random measurement uncertainty a fleet of 20 aircraft is chosen. For each aircraft, the deviations of left wing and right wing measurements are used to determine estimates of the random measurement uncertainty. A comparison of the analysed standard deviations reveals different results between the uncertainties derived with different engine pairs. These observed differences exceed the 95% confidence intervals which are, calculated as per [18], below  $\pm 5\%$  of the analysed standard deviations. They are due to non-constant phenomena, other than the random measurement uncertainty, that are not filtered out. Non-detected outliers or step changes in the trend, for example, may result in a higher standard deviation for the data of some engine pairs. However, as a conservative approach, the highest value between the 20 analysed standard deviations of an engine parameter's measurement is selected as the overall estimation of the random measurement uncertainty.

The estimated random measurement uncertainties for the engine instrumentation are shown in figures 5.9 and 5.10 alongside reference values taken from uncertainty requirements for development instrumentation. It is to be kept in mind, that development instrumentation is commonly subject to more stringent requirements for measurement accuracy than production instrumentation. The reference values herein are stated to provide a comparative indicating whether or not the orders of magnitude of the analysis results are plausible. It is noted that for the different sensors, there is no one common ratio for systematic vs. random uncertainty. Data presented in [71], for example, shows random uncertainty to have a share of 12-95% of the total uncertainty.

For the majority of the parameters of figures 5.9 and 5.10, it is observed that the analysed random measurement uncertainties are lower than the reference values. This is



due to the latter being requirements for total measurement uncertainty. Analysed values are thus lower than the reference ones, in spite of measurements from development instrumentation being generally more accurate than those from production instrumentation. This effect is most pronounced for the  $p_5$  measurement whose pressure probes outnumber those of the other measurements. Prominent exceptions are the measurements of  $p_{25}$  and  $p_{125}$  where the analysed random measurement uncertainty exceeds the reference values. For the former, this result is supported by engine monitoring diagnosis experience with the given engine type, which showed this measurement to be less accurate than  $p_{25}$  measurements in other engine designs. For the  $p_{125}$  measurement, an explanation is given by a constructive particularity of the design of the engine used for this investigation. Air from the  $p_{125}$  sense line is also used for cooling of electronic components of the engine. This causes an increased uncertainty in the pressure measurement. It is furthermore observed that temperatures measured at elevated temperature levels, namely  $T_3$  and EGT, have higher uncertainties than temperatures measured in the colder engine sections. This is expected as measurement uncertainty at high temperatures is typically proportional to the temperature [16].

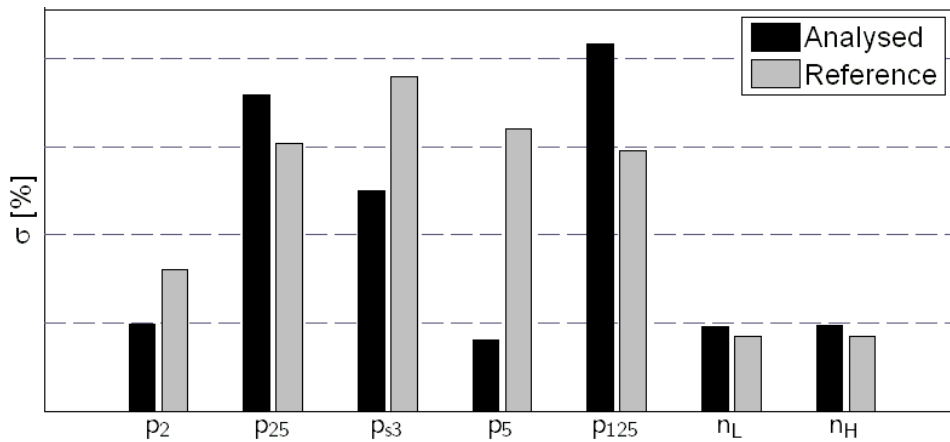


Figure 5.9: Analysed measurement uncertainty of production instrumentation (random) and reference values from development instrumentation requirements (random & systematic)

It is concluded that the analysis provides plausible results. The obtained values are used for the assessment of the uncertainty of performance recovery analysis.

Random measurement uncertainty of the aircraft-measured pressure and temperature are estimated analogously to the method applied to engine sensors. As there is only one measurement on the aircraft, the deviation is calculated with the respective engine inlet measurement. For the temperature, for example, the deviation  $T_0 - T_2$  is calcu-

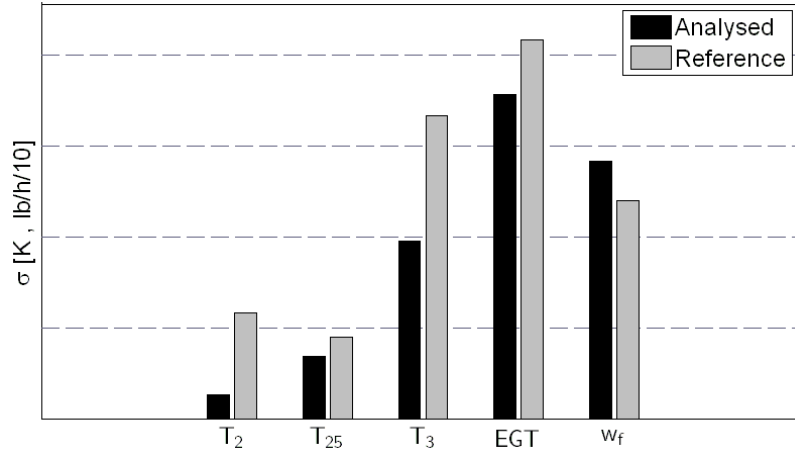


Figure 5.10: Analysed measurement uncertainty of production instrumentation (random) and reference values from development instrumentation requirements (random & systematic)

lated. A comparison of the two different measurements requires for actual conditions between the measurement plains of the Pitot tube and the engine inlet to be constant. Engine inlet temperature maybe considered equal to free stream temperature [32], a comparison is thus sensible. Pressure losses do occur alongside the aircraft fuselage, as well as within the engine intake. For a given dynamic pressure, the pressure loss of the engine intake may be considered constant [72]. For the aircraft, pressure losses are dependent on flight speed. To render variations of the pressure losses negligible, only data with similar operating conditions is therefore used.

Raw data is filtered for outliers and processed to include only data points with small variations of engine operating conditions. Filtering for unusual engine settings or accounting for engine deterioration is not necessary for inlet and aircraft measurements. Aircraft and engine measurements are obtained with different hardware. Using the random measurement uncertainty of the engine inlet measurement, obtained as per equation 5.12, the random measurement uncertainty of the free flow parameter is estimated with the law of error propagation:

$$\sigma_{\mathcal{R}_0} \approx \sqrt{S_{\Delta\mathcal{R}_{0-2}}^2 - \sigma_{\mathcal{R}_2}^2} \quad . \quad (5.13)$$

Analysed random measurement uncertainties of the aircraft's speed and temperature measurements are higher than the respective measurements at the engine inlet. For a measurement selection for the performance recovery analysis, however, the stochastic part of the remaining systematic uncertainty needs to be considered, as well.

### 5.2.3 Field Data-Based Assessment of the Stochastic Part of the Remaining Systematic Measurement Uncertainty

Measurements of engine inlet conditions and free flow conditions are subject to a change of the stochastic part of the remaining systematic uncertainty. With data being collected only during non-turbulent flight conditions, actual engine inlet conditions are the same for left and right wing engines. For the measurements, systematic differences are however observed when comparing engine inlet measurements of the two sides. The observed differences are the stochastic part of the remaining systematic uncertainty after calibration. By comparison of measurement data for an engine pair of one aircraft, a mean difference is calculated when averaging multiple snapshots:

$$\overline{\Delta\mathfrak{R}_2} \neq 0 \quad . \quad (5.14)$$

Raw data is filtered for outliers and processed to include only data points with small variations of engine operating points, as discussed in section 5.2.2. Filtering for unusual engine settings or accounting for engine deterioration is not necessary for inlet measurements. Calculation of the mean difference is repeated for multiple engine pairs, yielding  $S_{\overline{\Delta\mathfrak{R}_2}}$ , the normal distribution's standard deviation of the mean difference. The standard deviation of the stochastic part of the remaining systematic measurement uncertainty for a single measurement is, in an analogous manner to equation 5.12, derived as:

$$\sigma_{sys,\mathfrak{R}_2} \approx \frac{1}{\sqrt{2}} \cdot \sigma_{\overline{\Delta\mathfrak{R}_2}} \quad . \quad (5.15)$$

For the assessment of the stochastic part of the remaining systematic measurement uncertainty of aircraft instrumentation, aircraft measurements are compared to one of the inlet measurements. The resulting standard deviation of the mean difference  $S_{\overline{\Delta\mathfrak{R}_{amb-2}}}$  is used to estimate this stochastic part. With  $\sigma_{sys,\mathfrak{R}_2}$ , obtained as per equation 5.15, the estimation is derived analogously to equation 5.13:

$$\sigma_{sys,\mathfrak{R}_0} \approx \sqrt{S_{\overline{\Delta\mathfrak{R}_{0-2}}}^2 - S_{\overline{\Delta\mathfrak{R}_2}}^2} \quad . \quad (5.16)$$

Taking into consideration both the random measurement uncertainty and the stochastic part of the remaining systematic uncertainty, temperature measurement from the

aircraft is found to be less precise than that of the engine inlet temperature. For the pressure measurement, the aircraft measurement is found to be more precise than the engine one. This is to be expected as aircraft altitude and speed measurements, both of which are critical for flight safety, are highly sensitive to pressure measurements. Aircraft pressure measurement and engine inlet temperature measurement are therefore selected as the measurements used for performance recovery analysis.

### 5.2.4 Requirement-Based Assessment of Maximum Permissible Mach Number Measurement Uncertainty

Measurement uncertainty of the Mach number cannot be derived based on field data. Therefore, an estimate is established based on certification requirements. Mach number measurement is required to have a tolerance of  $\pm 0.005$  at standard cruise conditions in order to obtain aircraft certification [57]. With tolerances generally indicating maximum permissible deviations [29], this requirement is therefore taken as the upper limit for the measurement's  $3\sigma$  variations. Maximum permissible values for the random measurement uncertainty and the stochastic part of the remaining are thus given by [44]:

$$0.005 = \sqrt{(3\sigma_M)^2 + (3\sigma_{sys,M})^2} \quad . \quad (5.17)$$

Given this interval, the stochastic part of the remaining systematic measurement uncertainty and random measurement uncertainty can be calculated if their ratio

$$\lambda = \frac{\sigma_{sys,M}}{\sigma_M} \quad , \quad (5.18)$$

is known. The random measurement uncertainty then becomes:

$$\sigma_M = \frac{0.005}{3 \cdot \sqrt{\lambda^2 + 1}} \quad . \quad (5.19)$$

The ratio of the stochastic part of the remaining systematic measurement uncertainty to random measurement uncertainty is known for the free flow pressure based on the assessments of sections 5.2.2 and 5.2.3. Assuming that the measurement of free flow pressure respectively the differential pressure between total and static conditions has

the same ratio, Mach number measurement uncertainties will also be of equal ratio. Due to the non-linear relation between pressures and Mach number, the mathematical demonstration for this conclusion is given in appendix A.1. The assumption of the pressure measurements having an equal ratio of the stochastic part of remaining systematic measurement uncertainty to random measurement uncertainty needs to be substantiated. It is made considering that aircraft pressure measurements are typically part of one hardware set, a Pitot pressure tube with dedicated electronics. All elements of the measurement chain are from the same supplier and therefore of identical design. The ratio of uncertainties is thus considered equal.

With the given random measurement uncertainty, the stochastic part of the remaining systematic uncertainty is calculated with equation 5.18. The results of this assessment are maximum permissible limits for the uncertainties. Aircraft hardware is potentially more accurate than defined in the certification requirements. Furthermore, the remaining systematic uncertainty may contain a non-zero constant part.

## 5.2.5 Test Cell Measurements

Uncertainty of test cell measurements is assessed to enable a comparison of the accuracy of performance recovery analysis based on monitoring data with one based on test cell data. Performance recovery analysis based on test cell data can be carried out where optional test cell runs are carried out at the incoming stage of the engine shop visit. Performance analysis based on test cell data is generally considered to be more accurate but is often not an option due to the high costs, increase in TAT and constraints on test cell availability associated with incoming engine runs [22]. Performance data collected during test cell runs includes all parameters of the engine instrumentation. Furthermore, both additional parameters and parameters redundantly measured to the ones available in engine instrumentation are recorded. Parameters measured in the test cell are:

- engine thrust  $F$  (additional);
- total engine inlet flow  $w_2$  (additional);
- relative humidity  $\varphi$  (additional).
- spool speeds  $n_L$  and  $n_H$  (redundant);
- fuel flow  $w_f$  (redundant).

With the necessary specifications available, an uncertainty analysis as discussed in [31] and [2] is carried out. Due to the superior accuracy of test cell instrumentation compared to engine instrumentation, the former is used to assess the uncertainty of performance recovery analysis with test cell data.

## 5.3 Model Uncertainties

Errors of the performance model constitute the second major source for inaccuracy of the analysed performance recovery. Engine operation with engine settings which deviate from the nominal settings for which the engine model setup, is one such source. With monitoring data indicating only high flow or nominal flow setting of the bleed valve, for example, the increased mass flow for the high flow setting cannot be quantified in the engine model. The impact on analysis uncertainty is therefore decreased by filtering out engine data with high flow setting. Non-nominal VSV settings and power extraction are filtered out analogously. The impact of numerical precision of the data collection and analysis process is negligible [39].

Not all sources of model uncertainties can be considered negligible for all analysed components or may be reduced by filtering. These error sources are quantified. Some of the discussed errors are due to installation effects and will apply only to the use of on-wing data but not for test cell performance runs. Others do have an impact on analysis uncertainty regardless of the data source.

### 5.3.1 Fuel Heating Value

Actual Fuel Heating Value (FHV) for a given flight is not measured. It is therefore assumed to be a nominal, constant value set within the engine model. This is in disagreement with reality where the FHV varies from flight to flight as each airport has its own supplier, in some cases even multiple ones. Furthermore, variations may occur between deliveries from the same supplier due to variations in the oil quality and the refining process. Variations of the FHV induce also a model uncertainty for performance recovery analysis based on test cell data. Unlike in development testing, FHV is not measured with lab tests for test cell runs of overhauled engines. Variation of the actual FHV is approximated by a Gaussian distribution with  $\sigma = 0.31\%$  as displayed in fig. 5.11. It is noted that FHV is constraint by a lower value, 42.8 MJ/kg for Jet A1 [1].

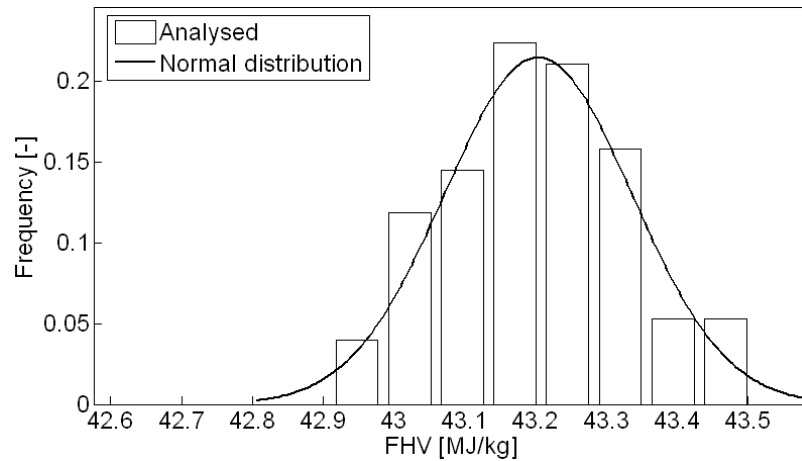


Figure 5.11: Distribution of FHV for airline operation as per US Department of Energy survey [40]

### 5.3.2 Exhaust Nozzle Exit Area

Maintenance schedules of the engine exhaust nozzles are independent from the powerplant. As overhauled engines are typically not installed to the same aircraft they were installed on prior to the shop visit, an engine shop visit results in a change of the nozzle-powerplant combination. This means for the powerplant to be matched with nozzles of different exit area prior to and following its shop visit, causing a different mass flow. These changes are not integrated in the engine model when analysing monitoring data as unit specific information on the nozzle geometry is unknown.

In [4], the impact of manufacturing procedures on exhaust nozzle capacity of new engines is investigated. The capacity standard deviation is quantified as  $\sigma = 0.43\%$  based on statistical evaluations off pass-off data. The impact of measurement uncertainty on the analysis result is not extracted. Therefore, reference values for measurement uncertainty at the exhaust nozzle exit plain are taken from [60]. The measurement uncertainty for the indirectly measured capacity is quantified as  $\sigma = 0.38\%$ . The actual capacity variation, which is assumed to be due to area variation, is therefore calculated as  $\sigma = 0.21\%$  based on the law of error propagation.

### 5.3.3 Thrust Reverser Leakage

Leakage mass flow of the thrust reverser changes when installing the powerplant to another airplane, as the nacelle is a different one. Changes of leakage are not incorporated into the engine model for analysis with monitoring data due to a lack of information

on unit specific leakage flow. This causes an error in bypass mass flow analysis.

It is assumed that leakage of thrust reversers varies from zero for a new or freshly overhauled unit to a maximum value seen on units at the end of their overhaul cycle. In [78], an increase of the SFC of up to 1% is attributed to the use of thrust reverser due to pressure loss and maximum leakage during operation. Based on cruise condition synthesis calculations and the quantification of nacelle pressure loss mechanisms presented in [25], it is assumed that the increase in SFC is divided into 0.34% due to pressure loss and 0.66% due to leakage flows. For the engine type used in the course of this research this translates into a maximum leakage of 0.33% of the bypass mass flow.

### 5.3.4 Water Content of the Ambient Air

The water content of the ambient air sucked in by the engine may appear in all three phases, as gaseous humidity, liquid rain or solid hail. Changes of the air's water content have an effect on both the gas constant as well as the isentropic exponent [36]. These changes are not integrated in the analysis of monitoring data as measurements of the local humidity, rain or hail is not available during flight. Instead, water content of the air is set to a constant value in the engine model. For the present model, water content is set to 0.

In [36] it is recommended that humidity effects on performance need only to be taken into account for Water-to-Air-Ratios (WAR) above 0.005. In comparison, saturated air at 10km cruise altitude and a temperature 20K above standard day conditions has a WAR of only 0.0009. Humidity effects are therefore considered negligible for cruise condition, an assumption verified by the findings presented in [39].

For rain, it is reported in [34] that even in the tropics, during the most rainy month, WAR at 11km altitude will reach its maximum value of 0.023 only about 0.1% of the time. It is furthermore stated that, during the worst month at the worst location, the probability of encountering hail of any size at 10.67km altitude is 0.067%. Based on these findings, rain and hail effects on performance are considered negligible for cruise operation in the relevant, non-tropic environment.



### 5.3.5 Booster and HPT Capacity Recovery

The applied statistical approach for modelling booster and HPT capacity recovery when using either component for core flow analysis induces a model uncertainty. Causes for the uncertainty are:

- engine-specific deviations from the model's mean capacity recovery;
- uncertainty of the model's mean capacity recovery.

A statistical quantification of engine-specific deviation from the true mean capacity recovery is derived with the sample engines used for establishing the statistical model discussed in chapter 5.1. The standard deviation of their analysed performance recovery,  $S_{\Delta w_{red,an}}$ , is calculated.

Uncertainty of the model's mean capacity recovery is due to the finite number of samples of the fleet data. As per central limit theorem, the distribution of an infinite number of sample means has, for a sample size  $N$ , a standard deviation [44]:

$$\sigma_{\mu} = \frac{S}{\sqrt{N}}. \quad (5.20)$$

The uncertainty of the model's mean capacity recovery is thus given by its standard deviation. It is quantified as  $\frac{S_{\Delta w_{red,an}}}{\sqrt{N}}$ .

### 5.3.6 Secondary Air System

The SAS is an uncertainty source for the analysis of component performance recovery. The uncertainty is due to:

- a variation of bleed mass flows from the compressor to the external air system;
- a variation of air mass flow at off-takes and feeds between the engine gas path and the engine's internal air system.

With the constraint of nominal bleed flow settings and small variations of the engine operating conditions, variation of bleed flow to the external air system is negligible [75].

Variation of the mass flows between gas path and internal air system can be both due to changed seal clearances and to blockage of the turbine blades' cooling holes.

The latter is considered to be negligible for this investigation. Maintenance records showed no cooling hole blockage for this investigation's fleet. An explanation for this circumstance is given by the engines not being operated in sandy environment.

For an assessment of mass flow variation due to changed seal clearances, clearance-to-mass-flow exchange rates for the HPC given in [55] were used. Bleed air flows extracted from the booster are neglected due to their low order of magnitude [43]. These exchange rates have been established based on the same engine used for this investigation. Using the exchange rates and maintenance-induced statistical variations of seal clearances, deduced from maintenance records, variations of the mass flow were calculated. For the two off-takes most sensitive to seal clearance changes, a decrease of the mass flow of 1.6% and an increase of mass flow of 0.4% respectively are found. The implications on performance analysis uncertainty are shown in table 5.4. An impact is observed only on HPC efficiency and both HPT performance parameters. HPT efficiency is most sensitive. The induced analysis error is, however, still below one per mil.

Mass flow change at ...	Fan		Booster		HPC		HPT		LPT	
	$\eta$	$w_{red}$	$\eta$	$w_{red}$	$\eta$	$w_{red}$	$\eta$	$w_{red}$	$\eta$	$w_{red}$
both ports	0.00	0.00	0.00	-	-0.02	0.00	0.09	-0.08	0.00	0.00

Table 5.4: Analysis error (per cent) induced by a 1.6% decrease and 0.4% increase respectively of the HPC's two air off-takes most sensitive to clearance changes of the internal air system

Variation of the air mass flow at off-takes and feeds induce also turbine performance changes which cannot be simulated with performance calculations. These are [68]:

- a decrease of the specific enthalpy and a pressure loss due to the mixing process of cooling air and the main air flow of the gas path;
- performed pumping work of the radial cooling air flow within the rotor blades.

Based on the exchange rates of turbine efficiency to a variation in feeding air mass flow, as per [68], and the calculated maintenance-induced changes of the mass flow, the non-simulated efficiency change of the two-stage HPT is assessed. It is found to be below 0.5 per mil. Overhaul of the SAS is therefore considered to cause a negligible uncertainty in performance recovery analysis for turbo components.

### 5.3.7 Engine Settings

Engine settings that are not covered in the previous sections may cause further uncertainty of component analysis. This is due to a missing model of a setting's impact on component behaviour. Engine settings that impact performance and have not yet been discussed are settings of the VSV system and power extraction. Their impact on the uncertainty of analysed performance recovery is minimised by filtering out snapshots with unusual engine settings. Any error made in the analysis is therefore constant for all snapshots. The impact when comparing performance prior to and following a shop visit is thus considered negligible.

## 5.4 Simulation of Performance Recovery Analysis Uncertainty

### 5.4.1 Monte Carlo Simulation

Due to the iterative process of modular performance calculation the analysis uncertainty cannot be derived analytically with the given model. A possible approach for calculating the effect of statistically distributed parameters on engine performance problems is the use of a Monte Carlo Simulation [65]. In figure 5.12, a scheme of a used Monte Carlo Simulation of this investigation is shown.

The aim is to simulate analysis uncertainty due to random measurement uncertainty of engine production instrumentation. Input variables for the analysis are generated by overlaying nominal values for each measured parameter, representative of an average cruise operating point, with distributions describing the random measurement uncertainties derived in section 5.2.2. Random values are pre-processed by rounding to the digit precision available in transmitted on-wing data. The rounded values are used as input for performance analysis using GPA. The calculation is repeated  $n$ -fold until both the random input parameters and the calculated output parameters have resumed stable mean values and standard deviations. The values are assumed stable and a satisfactory approximation of the true mean and standard deviation if their relative rate of change remains below 0.1% for 500 consecutive calculations. 6000 calculations are needed to satisfy this criterion [38]. Analysis uncertainty due to the stochastic parts of the remaining systematic measurement uncertainties is simulated analogously to the setup shown in figure 5.12. In order to compare different core flow analysis methods,

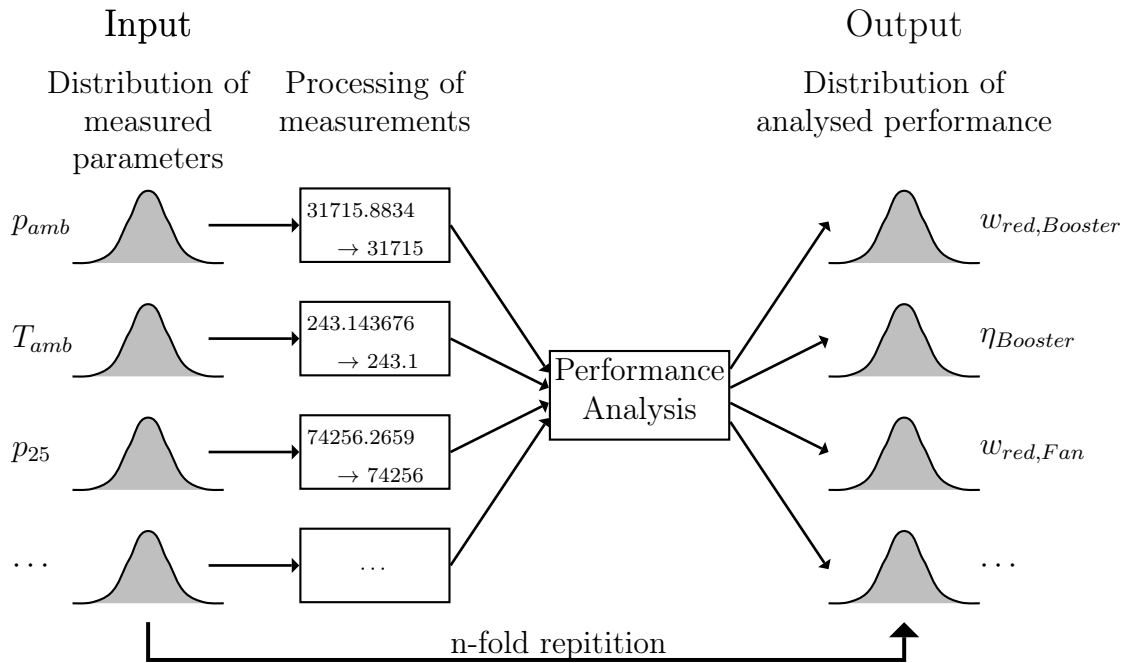


Figure 5.12: Schematic illustration of the Monte Carlo Simulation setup used for assessing analysis uncertainty due to random measurement uncertainty

the Monte Carlo Simulations are each carried for the:

- booster capacity method;
- HPT capacity method;
- LPT capacity method.

Analysis uncertainty due to model uncertainties is also simulated using Monte Carlo Simulations. A scheme of the setup used for simulating the effect of exhaust nozzle area variation on analysis uncertainty is shown in figure 5.13. A cruise operating point, representative of average operating conditions, is used for synthesis calculation. Exhaust nozzle exit area of the synthesis model is varied about its nominal value according to the magnitude given in sections 5.3.2. The output of the synthesis calculation is used as generic data for an analysis calculation. Nozzle area of the analysis model is set to its nominal, constant value, as would be the case for analysis of actual monitoring data. The analysis yields distributions of component performance parameters as the overall output of the Monte Carlo Simulation. As for the measurement induced uncertainties, the simulation is repeated for all three core flow analysis methods. Simulations for uncertainties in FHV and thrust revers leakage are carried out analogously. For modelled recovery of booster and HPT capacity, only the respective core flow analysis method

is used for the simulation.

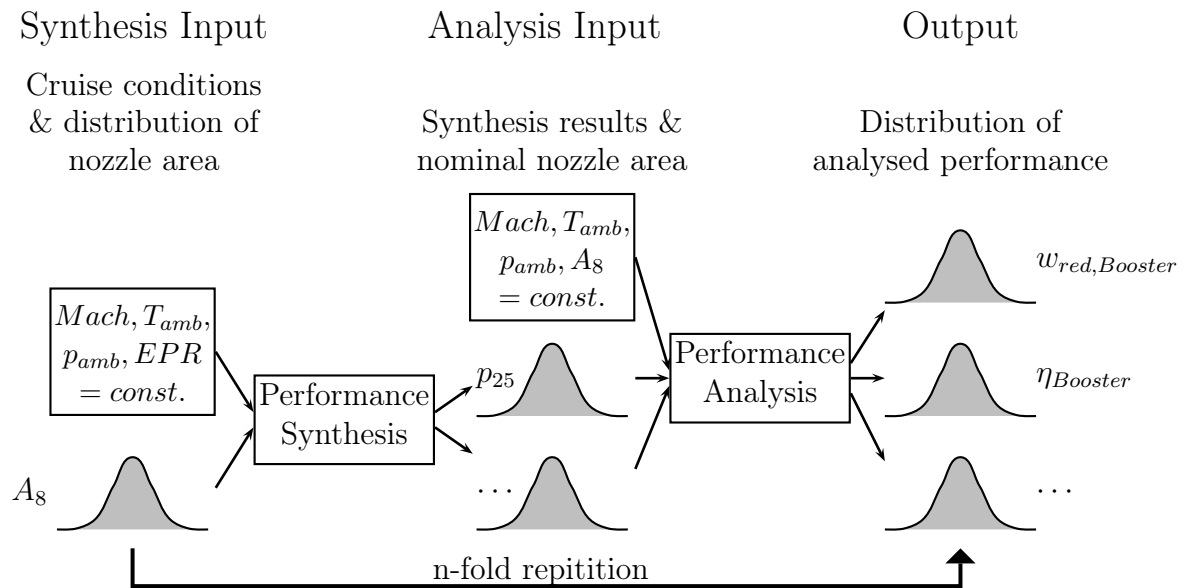


Figure 5.13: Schematic illustration of the Monte Carlo Simulation setup used for assessing analysis uncertainty due a variation of the exhaust nozzle exit Area ( $A_8$ )

Generally, the uncertainties of measurements and engine model lead to variations in analysed results. As an example, results of the uncertainty calculation for exhaust nozzle exit area variation are shown in table 5.5. Booster capacity and HPT capacity method yield lower variations for the core components' characteristics than analysis through LPT capacity method. Furthermore, effects on booster and HPC parameters, as well as on HPT capacity are small. It is observed that, between the core components, analysis of the LPT's efficiency is most sensitive to nozzle area variation with an uncertainty of up to 1.26%. This is explained by the fact that LPT efficiency is analysed using the power balance on the low pressure spool which depends on the bypass mass flow. Compressor capacities and HPT characteristics are most sensitive to the use of the LPT capacity method. This is to be expected as total engine mass flow, which is analysed with nozzle capacity characteristics, has a strong impact on core mass flow for this method.

The Monte Carlo simulations as described above are repeated for the test cell case. Additional measurements available in the test cell and improved accuracies of redundant measurements are considered in the model setup. Typical test cell operating conditions are used for the simulation. Uncertainties due to installation effects which apply only to on-wing monitoring data are not simulated.

Core flow analysis method	$U_{95}$ [%]									
	Fan		Booster		HPC		HPT		LPT	
	$\eta$	$w_{red}$	$\eta$	$w_{red}$	$\eta$	$w_{red}$	$\eta$	$w_{red}$	$\eta$	$w_{red}$
Booster capacity	1.38	0.95	0.00	-	0.00	0.00	0.13	0.01	0.44	0.29
HPT capacity	1.39	0.96	0.00	0.01	0.00	0.01	0.13	-	0.45	0.30
LPT capacity	0.74	0.51	0.00	0.48	0.04	0.50	0.38	0.33	-	-

Table 5.5: Standard variation of analysed component performance due to nozzle exit area variation and used core flow analysis method

### 5.4.2 Assessment of Total Analysis Uncertainty

Based on the simulated uncertainties of chapter 5.4.1, total uncertainty of performance recovery analysis can be derived. In order to calculate total uncertainty, it is to be considered that the simulated uncertainties are of three different types:

- random uncertainties due to snapshot variations ( $\sigma$ );
- stochastic part of systematic uncertainties due to installation distributions ( $\sigma_{sys}$ );
- stochastic part of systematic uncertainties due to pre-to-post overhaul changes ( $\sigma_{sys,\Delta}$ ).

An overview, which uncertainty type the simulated effects are, is given in table 5.6. For the latter type, the simulated uncertainty is tantamount to uncertainty of analysed performance recovery due to a single effect. For the former two, the uncertainty of the performance recovery needs to be derived analytically based on the simulated uncertainties. The derivation is given exemplary for the efficiency in the following. Capacity recovery is calculated analogously.

Effect	Uncertainty is		
	random	system.	
	$\sigma$	$\sigma_{sys}$	$\sigma_{sys,\Delta}$
Nozzle area		x	
Thrust reverser		x	
Booster capacity			x
HPT capacity			x
Fuel Heating Value	x		
Measurement	x	x	

Table 5.6: Types of simulated analysis uncertainties per underlying effect

Efficiency recovery is calculated by comparing performance analysis prior to and following the shop visit:

$$\Delta\eta = \eta_{post} - \eta_{pre} \quad . \quad (5.21)$$

With the law of error propagation the uncertainty of performance recovery for a given  $\sigma_{sys}$  is derived as:

$$\sigma_{sys,\Delta\eta} = \sqrt{2} \cdot \sigma_{sys,\eta} \quad . \quad (5.22)$$

For random uncertainty, the uncertainty of performance recovery, when using one analysis point each prior to the shop visit and following it, derived analogously:

$$\sigma_{\Delta\eta} = \sqrt{2} \cdot \sigma_{\eta} \quad . \quad (5.23)$$

By averaging multiple snapshots the actual value of recovered performance may be approximated better as the impact of random errors is reduced [8]. However, when averaging multiple snapshots deterioration effects need to be considered. It is to be shown that the system in question, the engine, may be considered to be of constant state. For that purpose a  $\chi^2$ -homogeneity test is carried out. The test, described for example in [8], examines two or more sets of data with respect to their being of the same population or not. In the present case a number of 50 valid snapshots is tested for their being part of a constant engine state. For that purpose the first 25 snapshots are defined to constitute the first data set which is compared to the second data set comprising the snapshots 26 through 50. The test is carried out with field data from 134 engines. For all engines the last 50 valid snapshots before the engine shop visit and the first 50 valid snapshots after overhaul are subjected to a  $\chi^2$ -homogeneity test with a 99.9% confidence interval. Tested parameters are the efficiencies of HPC and HPT, both of which are, by experience, suspect to so-called 'running-in' effects. The results of the test are presented in table 5.7.

For the HPC efficiency prior to the shop visit, the  $\chi^2$ -test is successful for all but 2.2% of the tested engines. For the efficiency post shop visit, which is most critical for non-negligible deterioration rate, all engines pass the test. For the HPT efficiency prior to engine shop visit and following it, all engines pass the test, indicating a quasi-constant

	$\eta_{HPC}$		$\eta_{HPT}$	
	pre	post	pre	post
Failed $\chi^2$ -tests	2.2%	0%	0%	0%

Table 5.7:  $\chi^2$ -homogeneity tests with a 99.9% confidence for HPC and HPT efficiency for data of pre and post engine shop visit (50 snapshots each)

efficiency. This is attributed to the mandatory running-in procedure at the beginning of the pass-off test cell run. It is concluded that averaging 50 valid snapshots to describe the engine state before and after the overhaul is a valid approach.

With the uncertainties of performance recovery as per equations 5.22 and 5.23, the confidence interval for averaging efficiency with 50 measurements can be calculated. The uncertainty interval for 95% confidence, due to the uncertainty induced by a single effect, is then calculated as [5]:

$$U_{\Delta\eta,95} = \pm \sqrt{(t_{95,sys} \cdot \sigma_{sys,\Delta\eta})^2 + \left(\frac{t_{95}}{\sqrt{50}} \cdot \sigma_{\Delta\eta}\right)^2} \quad . \quad (5.24)$$

with  $t_{95} = f(N_{ref} - 1)$  as the student t-factor. The reference sample therein is the one used to calculate the standard deviation, in this case the Monte Carlo Simulation with a population size greater 6000. For a population of sufficient size ( $N_{ref} \geq 30$ ) the student-t factor for the 95% confidence interval is well approximated as 2 [5].

For the uncertainty calculation of performance recovery analysis using test cell data, equation 5.24 is applied with  $N = 1$ . A complete overview of the single effects' confidence intervals for the on-wing and the test cell case is given in appendix A.2. With the confidence intervals for all single effects, as listed in table 5.6, the total confidence interval for performance recovery analysis is:

$$U_{\Delta\eta,95} = \pm \sqrt{\sum_i U_{\Delta\eta,95,i}^2} \quad . \quad (5.25)$$

A comparison of different effects shows that few are responsible for the majority of a performance parameter's analysis uncertainties. As an example, an overview of total accuracy for the analysis of recovered HPC efficiency using the booster capacity method, is shown in figure 5.14. Total uncertainty of  $\pm 0.15\%$  is primarily attributed to non-observable changes in booster capacity and measurement uncertainty. Given a



correlation that accurately models the capacity change based on hardware information, the best possible uncertainty which can be realised for the analysis of HPC efficiency recovery is  $\pm 0.09\%$ . Performance changes of smaller magnitude are not observable.

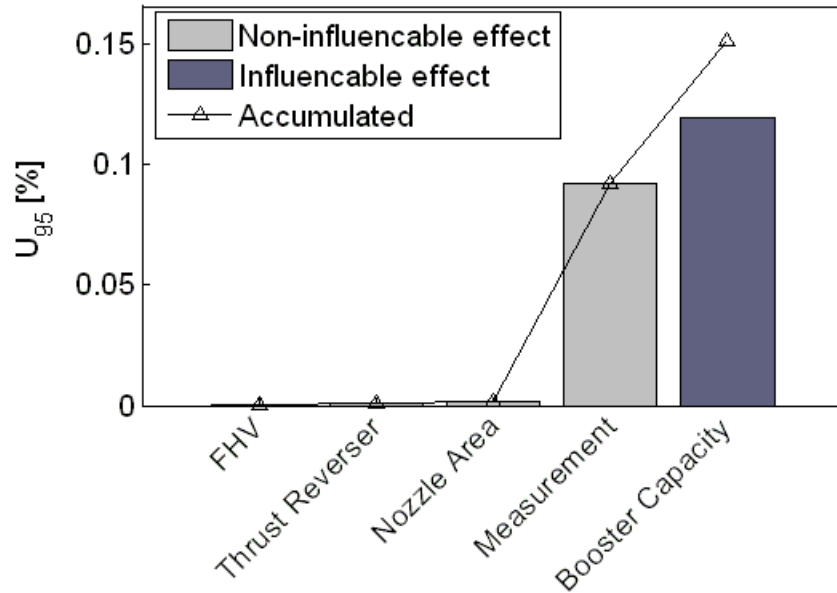


Figure 5.14:  $U_{95}$  for analysed HPC efficiency recovery with on-wing data using the booster capacity method

Uncertainty of analysed HPT efficiency recovery, when using booster capacity for analysing the core mass flow, is shown in figure 5.15. HPT efficiency analysis is more inaccurate than that of the HPC. Total uncertainty is  $\pm 1.18\%$  including all effects. Through improvements of the analysis model total uncertainty can theoretically be reduced to  $\pm 0.35\%$ . A maximum possible reduction by a factor of 3.4 is therefore possible. For the HPC efficiency uncertainty, as discussed above, the maximum possible improvement factor is 1.4.

The use of on-wing data for the purpose of analysing component performance recovery is to be compared with the use of test cell data. An overview of total uncertainty, using the LPC capacity method for core flow analysis, is given in table 5.8. Analysis of the booster and high pressure components' efficiencies is more accurate using on-wing data. This is explained by the improved analysis accuracy brought about by averaging multiple snapshots with on-wing data. Capacity changes of the high pressure components are more accurately analysed with test cell data. The relative gain in accuracy is, however, small. Fan and LPT, both of whose analysis is more sensitive to installation effects, are more accurately analysed with test cell data. Given the magnitude of the difference, an additional test cell run prior to engine disassembly is beneficial only for

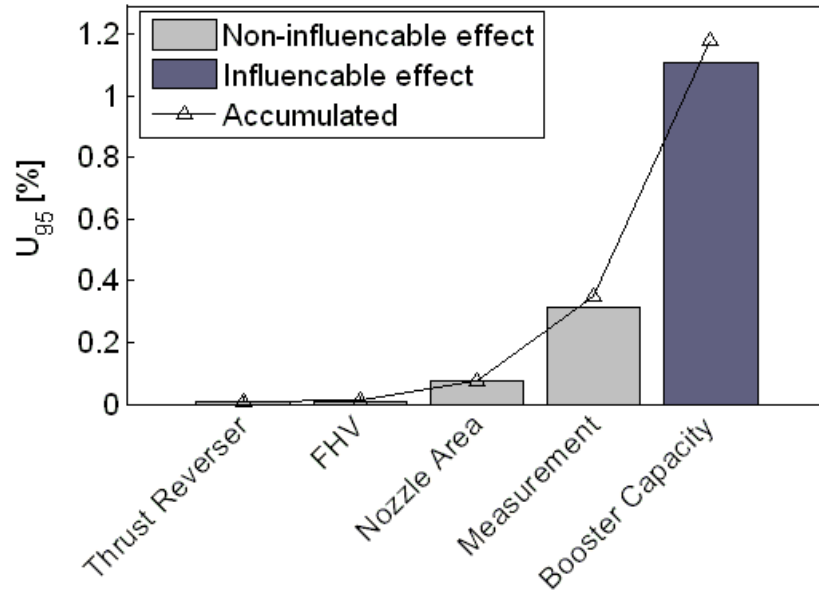


Figure 5.15:  $U_{95}$  for analysed HPT efficiency recovery with on-wing data using the booster capacity method

assessing an overhaul induced performance effect on these components. When comparing uncertainties obtained with the HPT and LPT capacity method respectively, the conclusions reached are the same as with the booster capacity method.

	$U_{95}$ [%]									
	Fan		Booster		HPC		HPT		LPT	
	$\eta$	$w_{red}$	$\eta$	$w_{red}$	$\eta$	$w_{red}$	$\eta$	$w_{red}$	$\eta$	$w_{red}$
On-wing data	5.02	3.46	1.41	-	0.15	2.30	1.18	1.51	2.50	1.66
Test cell data	0.82	0.56	1.79	-	0.85	2.13	1.32	1.38	1.34	0.89

Table 5.8:  $U_{95}$  (total uncertainty) for analysis based on on-wing and test cell data using the booster capacity method

## Chapter 6

# Correlation of Overhaul Workscope and Effect

### 6.1 Correlation Process

For the correlation, the feature restoration model established in section 4.2 is enhanced by a function defining the impact of feature change on performance loss. In common practice, this functional relation is often described by a linear factor  $d_k$  [65]. In the case of the efficiency, one obtains:

$$\Delta\eta_k = d_k \cdot \Delta X_k \quad . \quad (6.1)$$

With equation 4.6, the expected performance recovery due to the degree of restoration of a feature  $k$  of a cluster  $n$  is thus modelled as:

$$\Delta\eta_{n,k} = \alpha_{n,k} \cdot \xi_{n,k} \cdot \max(0, t - t_{0,n,k})^{1/\gamma_{n,k}} \quad , \quad (6.2)$$

wherein the factor  $\alpha_k$  integrates the coefficients  $a_k$  and  $d_k$ , while  $\gamma_k$  corresponds to the coefficient  $b_k$ . Assuming linear independence of the multiple features impacting performance recovery, as proposed in [65], total recovered performance is calculated as:

$$\Delta\eta = \sum_{n,k} \alpha_{n,k} \cdot \xi_{n,k} \cdot \max(0, t - t_{0,n,k})^{1/\gamma_{n,k}} \quad . \quad (6.3)$$

In order to establish a model for the recovered performance specific to an engine type, the coefficients  $\alpha_{n,k}$ ,  $t_{0,n,k}$  and  $\gamma_{n,k}$  in equation 6.3 need to be quantified. Applying equation 6.3 to the field data of the available fleet of overhauled engines results in an indeterminate system of non-linear, discontinuous equations. There is thus neither an analytical, nor an unique solution for the coefficients. They are therefore approximated using an optimisation algorithm [54].

The optimisation problem consists of minimising the deviation between measured and predicted performance recovery on a whole-component basis, summed up across a fleet of p-subscripted engines constituting the field data base. For the recovery of the efficiency parameter  $\eta_{pred}$ , calculated with in equation 6.3, and the measured parameter  $\eta_{meas}$ , obtained per analysis as discussed in chapter 5, the target function can be defined. With the coefficients  $\alpha_{n,k}$ ,  $t_{0,n,k}$  and  $\gamma_{n,k}$  in matrix form, it becomes:

$$f(A, T_0, \Gamma) = \sum_p |\Delta\eta_{p,pred}(A, T_0, \Gamma) - \Delta\eta_{p,meas}| \quad . \quad (6.4)$$

Training of the model is achieved by minimisation of the target function through variation of the coefficients. Assuming only linear or digressive deterioration types, the optimisation is subject to the following boundary conditions:

$$\gamma_{n,k} \geq 1 \quad , \quad (6.5a)$$

as well as

$$\alpha_{n,k} \geq 0 \quad , \quad (6.5b)$$

$$t_{0,n,k} \geq 0 \quad . \quad (6.5c)$$

For the choice of the algorithm, the following requirements need to be met. The algorithm has to:

- be able to handle non-linear functions;
- be able to handle discontinuous functions;
- be able to handle multidimensional functions;
- operate without analytical function derivatives;

- offer the best compromise, between all algorithms meeting the above requirements, of computing time and robustness.

With the given requirements, the downhill simplex method [52] is selected as the used optimisation algorithm. As it does not allow to categorically exclude parts of the solution space, boundary conditions are set by adding a penalty function to the target function [28]. With the penalty function  $g(A, T_0, \Gamma)$  the enhanced target function becomes:

$$f_{enh}(A, T_0, \Gamma) = f(A, T_0, \Gamma) + g(A, T_0, \Gamma) \quad . \quad (6.6)$$

The penalty function takes on the value 0 if all independent variables are within the permissible boundaries. If not, it takes on a high value causing the enhanced target function to increase substantially and the optimisation algorithm to 'manoeuvre' out of the non-permissible solution space. For the implementation of the algorithm, the parameters which are to be optimised are normalised. The aim of normalisation is to have parameters of a similar order of magnitude thus allowing for an optimal performance of the algorithm.

## 6.2 Validation of the Correlation

For the validation, both the input data and the correlated model are assessed. Validation of the correlation is carried with two components. HPC and HPT are selected given their high potential for recovery of SFC [59], [58] and EGT-Margin [61]. The latter is typically used as the key performance indicator for engine health during operation or at overhaul pass-off testing. It has also become a key factor for contractual agreements between engine operator and the overhaul provider [22]. Selection of the HPC and HPT is furthermore based on the superior accuracy with which their performance recovery can be analysed in comparison to the other turbo components. As discussed in section 4.3, the HPC is clustered into a front and rear so as to evaluate workscope impact separately for each part. The considered features are based on the classification presented in table 4.2. For the HPT, the more recently developed repair of applying new coating to the blades is considered additionally. Re-coating of the airfoils includes a stripping of the old, partially burned coating and an application of a new and even layer, thus improving the blade surface.

### 6.2.1 Assessment of the Input Data

Input data is assessed with respect to the resulting model's validity range. For the assessment, the principle ideas of data sampling are used. Methods for assessing the validity range of the input data based on a continuously quantifiable value, do not exist. Latin Hypercube Sampling (LHS) is applied for the assessment. It uses the ideas of Latin square experimental design in order to eliminate confounding effects of an experiment's variables, if repetition of that experiment is to be carried out under a strictly limited number of different conditions for these variables [14]. The idea, as shown in table 6.1, is to guarantee that each variable's different ranges of values are represented, regardless of how important they turn out to be. For a problem with two variables, each divided into three possible ranges of values, this may be fulfilled by a threefold repetition of the experiment. The minimum requirement is met if each value range, in this case row or column, occurs at least once.

		Variable 1: range...		
		1	2	3
Variable 2: range...	1		•	
	2	•		
	3			•

Table 6.1: LHS sample with 2 variables and 3 value ranges each

In the present case, the input variables are the degrees of restorations for each feature and the time since last overhaul. For the degrees of restoration, two equally spaced intervals covering the possible range from 0% to 100% are defined. For the time since last overhaul, three equally spaced intervals are defined covering the range from 0 cycles to the maximum number encountered in the data set. An analysis of the workscope data of HPC and HPT shows there to be at least one sample point per plain in the multidimensional table. It is therefore concluded, that the input data is sufficiently well spread.

## 6.2.2 Assessment of the Correlated Model

In order for the model to be mathematically independent of the sought solution, that is to say to prevent over-fitting of the model, the test engines used for validation must not be part of the training set [46]. Due to the limited size of the fleet, the leave one out algorithm is used to decrease the size of the training set as little as possible, thus guaranteeing a minimal variance of the solution. The scheme of the implemented

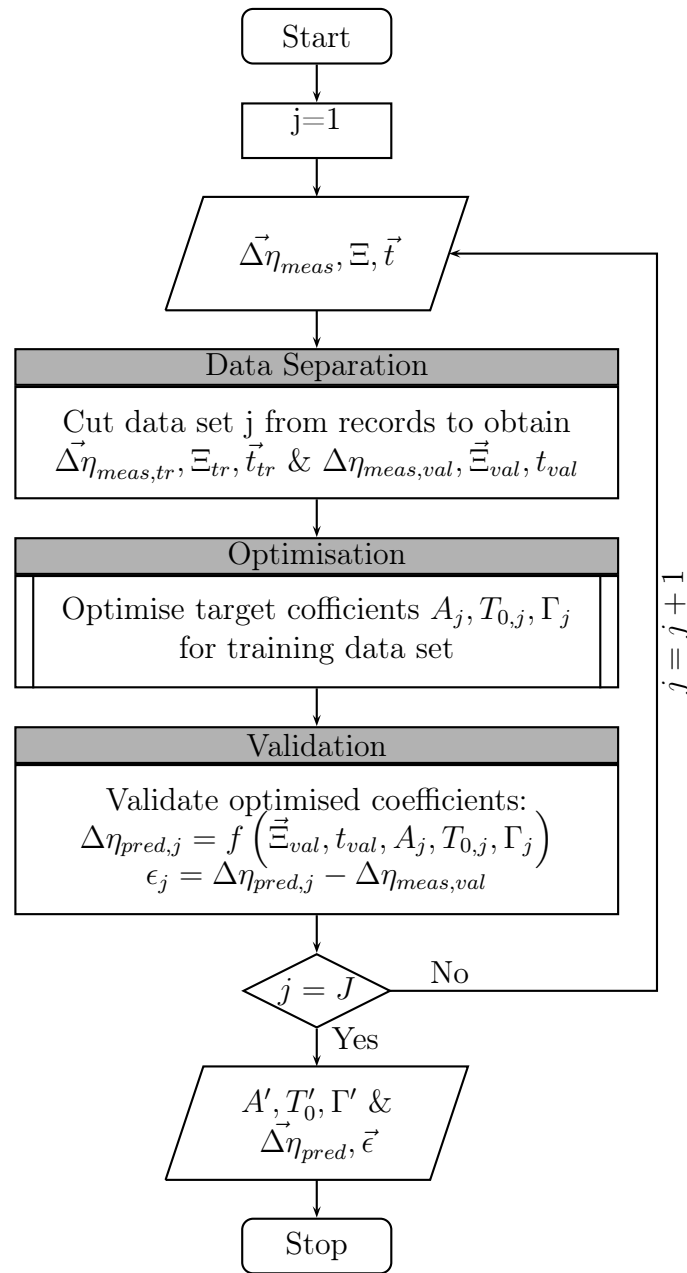


Figure 6.1: Scheme of a cross-validation loop for component efficiency recovery using the leave one out algorithm (LOO)

calculation sequence for the correlation of worksocpe and performance data is shown in figure 6.1. For a field data base of  $J$  overhauled engines, the algorithm takes as input the vector of the measured performance recovery, here  $\vec{\Delta\eta}_{meas}$ , the matrix  $\Xi$  defining the degree of restoration for  $K$  features of  $N$  clusters and the vector of operating time,  $\vec{t}$ . In a first step, one engine's data set, which is to be used for validation, is extracted leaving a reduced data base. The reduced data base is subsequently used for training of an optimised model correlating worksocpe and performance with the coefficient matrices  $A_j$ ,  $T_{0,j}$  and  $\Gamma_j$ , as discussed in section 6.1. The optimised model is then used to predict the recovered performance of the validation engine based on its degrees of restoration and operating time. In a final step, the predicted value is compared to the measured one, yielding the prediction's error  $\epsilon_j$ . This process is repeated  $J$  times, each time choosing another engine to be cut from the data base and to be used for training of the optimised overhaul model. The resulting output are the  $K \times N \times J$  matrices of the optimised models, as well as the corresponding vectors, of length  $J$ , for predicted performance recovery  $\vec{\eta}_{pred}$  and for the prediction error  $\vec{\epsilon}$ .

Results of the cross-validation for the HPC and HPT efficiency are shown in figures 6.2 and 6.3. Predicted and measured efficiency recovery are illustrated, including the 95% confidence interval about the line for zero deviation between measurement and

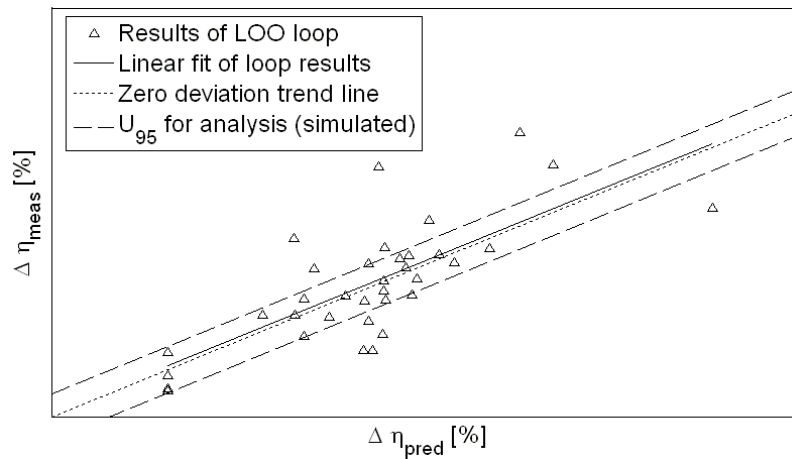


Figure 6.2: Predicted and measured HPC efficiency recovery for analysis using the booster capacity method

predictions. The confidence interval indicates the analysis uncertainty of the measured recovery value. It is quantified based on the results of the uncertainty simulation presented in section 5.4. It is observed, that the measured efficiency recovery deviates equally to both sides of the zero deviation trend lines. The slopes of the data's linear fit curves are quasi-parallel to that of zero deviation. The vertical offset is explained



statistically by the finite number of engines used for the cross-validation. Given the general trend of the cross-validation, the fit of the correlated models for HPC and HPT overhaul is concluded to be good.

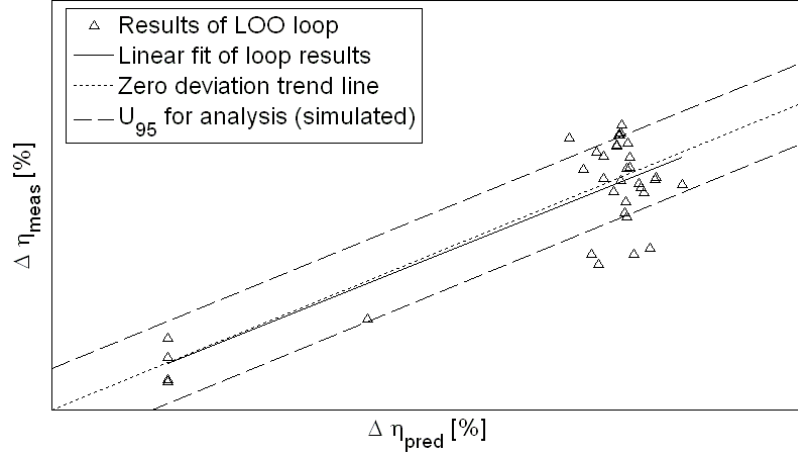


Figure 6.3: Predicted and measured HPT efficiency recovery for analysis using the booster capacity method

It is, however, observed from figures 6.2 and 6.3 that the scatter about the zero deviation curves exceeds that which is expected to be induced through the analysis uncertainty. The differences between simulated analysis uncertainties, observed model uncertainties and variations of the measured recoveries can be deduced from table 6.2. For the HPC, observed model uncertainty is at 0.62%. This is below the variation of the measured recovery which is 0.93%. However, the observed uncertainty is still above the simulated analysis uncertainty of 0.08%. Similar observations are made for the HPT. Observed uncertainty is at 1.12%, which is below the 2.09% variation of the measured performance recovery and above the 0.59% for simulated analysis uncertainty. It is thus concluded that the model improves the accuracy with which performance recovery of the HPC and HPT can be predicted. However, potential for a more accurate correlation remains.

	$\sigma_{\eta}$ [%]	
	HPC	HPT
Variation of measured recovery	0.93%	2.09%
Observed model uncertainty	0.62%	1.12%
Simulated analysis uncertainty	0.08%	0.59%

Table 6.2: HPC and HPT efficiency: measured variation, model uncertainty and analysis uncertainty using the booster capacity method

The differences between observed uncertainty and simulated analysis uncertainty are

explained by the former being due to uncertainty in both measured and the predicted efficiency. The increased scatter is thus attributed to the uncertainty of the abscissa's parameter  $\Delta\eta_{pred}$ . Uncertainty of the predicted efficiency recovery is, in parts, due the established model giving an expectancy of a probabilistic problem. As discussed in section 4.1, the model is set up to identify the mean potential for performance recovery. Furthermore, uncertainty of  $\Delta\eta_{pred}$  is due to:

- scatter about the mean value for the feature restoration for part repair or production of new parts;
- variations within the assembly process [41], [42];
- analysis uncertainty impact on the optimisation;
- uncertainty in the workscope data.

A maintenance process including the measuring of feature changes, due to engine overhaul and component assembly, is thus concluded to be indispensable for a more accurate correlation between overhaul workscope and performance recovery.

### 6.3 Application of the Methodology

The demonstrated correlation methodology is again applied to the HPC and HPT, in order to quantify the potential for performance recovery of the different features. The entire fleet data is used for training without extracting any data sets as done for the cross-correlation. The coefficients of the optimised correlation for the HPC are shown in table 6.3. The resulting potential for performance recovery with operating time,

	Restoration of ...							
	tip clearance (blade tip)		tip clearance (casing liner)		blade contour		surface roughness	
	Front	Rear	Front	Rear	Front	Rear	Front	Rear
$\alpha$ <sup>1</sup>	0.53	0.27	0.03	0.34	0.58	0.09	1.00	0.38
$t_0$ <sup>2</sup>	0.30	0.70	0.30	0.08	0.27	0.68	0.19	0.41
$\gamma$	5.62	5.84	7.63	7.33	6.10	5.21	6.17	6.62

Table 6.3: Optimised correlation factors for the impact of HPC front and rear part workscooping on efficiency recovery

<sup>1</sup>These coefficients have been normalised to the maximum value due to confidentiality reasons.

<sup>2</sup>These coefficients have been normalised to MTBSV due to confidentiality reasons.

quantified relatively to the Mean Time Between Shop Visits (MTBSV) of the used fleet, is shown in figure 6.4. It is observed that for blade features the potential is higher in the front stages, a fact reflected in higher  $\alpha$ -values. The difference between rear and front part is more pronounced for blade contour and surface roughness than for blade tip loss. For the blade features it is also observed that deterioration in the compressor front occurs after less engine operating time than it does in the rear.

Casing liner restoration is observed to have a higher potential for performance recovery in the HPC rear. Furthermore, distinct differences are observed to potential from tip clearance from the blade tip, reflected in different values for  $\alpha$  and  $t_0$ . The differences can be explained by dissimilar deterioration characteristics due to unequal materials for blades and casing. For all features, of blade and casing alike, the potential performance recovery shows a clearly digressive trend, quantified by the coefficients  $\gamma_{n,k} > 5$ .

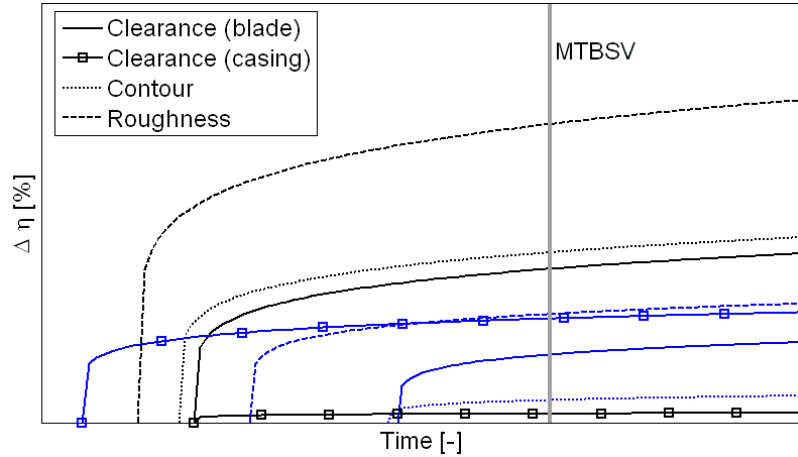


Figure 6.4: Potential for efficiency recovery with operating time for HPC features (for an equal degree of restoration  $\xi$ ); for front (black lines) and rear (blue lines)

Based on the correlation results it can be concluded, for the used engine, that the highest potential for performance recovery lies in restoration of the blade surface roughness, followed by blade tip clearance restoration. Restoration of blade contour is sensible only for the HPC front, while restoration of the casing liner is only sensible for the rear. Overhaul of blade features in the rear are generally sensible only for engines with a sufficient operating time. This information can be used by the maintenance provider to optimise overhaul workscope.

The coefficients of the optimised correlation for the HPT are shown in table 6.4. The resulting potential for performance recovery with operating time, again quantified relatively to the MTBSV of the used fleet, is shown in figure 6.5. A potential for performance recovery is observed only for clearance effects, not for the blade coating. The

latter can be explained by the type of the used fleet. As stated in section 5.1, the served network's environmental conditions are as typically found for a European or Northern American operator. Maximum temperatures and air contamination with sand are relatively low in these regions compared to operation in the Middle East. Stresses on the turbine hardware is thus lower, resulting in smaller damage of the blade surface or coating. For the present fleet this damage causes no observable change of the turbine efficiency and is therefore negligible. The optimised coefficients  $t_0$  and  $\gamma$  are, in the case of blade coating restoration, physically irrelevant results to a numerical problem.

	Restoration of ...			
	tip clearance (blade tip)	tip clearance (casing liner)	cavity clearance (seal fins)	blade coating
$\alpha$ <sup>3</sup>	0.00	1.00	0.64	0.00
$t_0$ <sup>4</sup>	0.08	0.01	0.44	0.17
$\gamma$	3.32	4.92	8.25	4.56

Table 6.4: Optimised correlation factors for the impact of HPT workscoping on efficiency recovery

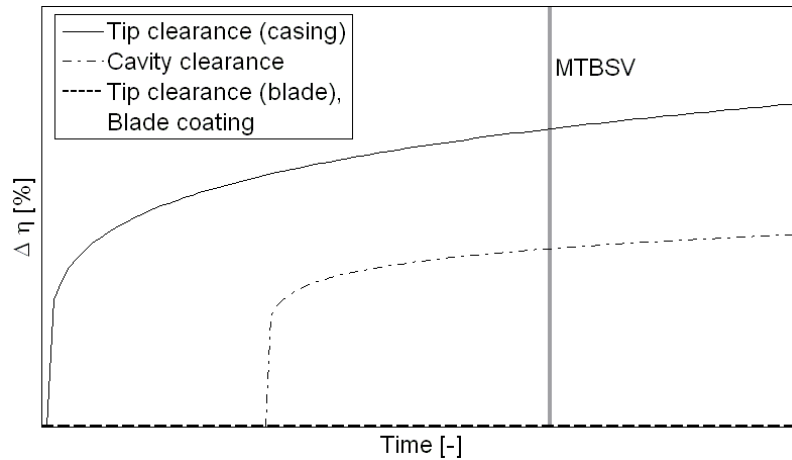


Figure 6.5: Potential for efficiency recovery with operating time for HPT features (for an equal degree of restoration  $\xi$ )

Recovery of the HPT efficiency can be realised both by restoration of the inter-stage cavity clearance and the clearance between blade tip and casing. For the latter, the correlation shows for tip clearance changes to be solely due to the casing liner. Between restoration of the casing liner and of the cavity clearance, the former is shown to have a higher potential for performance recovery. Quantitatively, this can be seen by

<sup>3</sup>These coefficients have been normalised to the maximum value due to confidentiality reasons.

<sup>4</sup>These coefficients have been normalised to MTBSV due to confidentiality reasons.

the higher exchange rate between degree of restoration and performance,  $\alpha$ , and the first deterioration occurring shortly after the beginning of operation, indicated by a lower coefficient  $t_0$ . In turn, cavity clearance is shown to be an interesting lever in guaranteeing remaining performance for a given period of operation following the shop visit. It is noted that, as for the blade coating, the optimised coefficients  $t_0$  and  $\gamma$  for blade tip restoration are physically irrelevant results to a numerical problem. As for the HPC correlation, the results of the HPT correlation provide clear levers for the maintenance provider to optimise engine overhaul workslope.



# Chapter 7

## Concluding Discussion

### 7.1 Summary

The increased importance of fuel consumption in the books of aircraft operators has led to a raised focus on the aspect of performance recovery for the engine overhaul process. It follows thus the need for a method to systematically and cost-efficiently investigate the impact of single workscope elements on engine efficiency.

A survey of existing studies and methods has unearthed recently developed methods for a comprehensive maintenance planning. These methods do not yet incorporate the aspect of performance recovery in spite of the high effort made to adapt engine specific workscope for observed hardware conditions. This is due to a lack of a systematic approach to establish a model correlating workscope and performance recovery. Research linking the two has so far been focused on predicting workscope-induced performance recovery based on predefined models and comparing the results with measured performance changes. No method for an adaptive model, based on available field data, has yet been established. Furthermore, any conceptual reflections to use field data to assess workscope impact on performance recovery are focused on the use of test cell data, rather than monitoring data recorded during engine operation.

To close this existing gap a new methodology has been developed, correlating the engine overhaul's workscope and its effect. The workscope has therein been defined by the degree of restoration which quantifies the percentage of parts for which a given feature is restored, either by repair or use of new parts. In order for the correlation model's extend to be manageable, the degree of restoration in components with high stage numbers has been defined for clusters comprising multiple stages.

The workscope effect, in terms of performance recovery, can be analysed using test

cell or on-wing data both of which are subject to uncertainty induced by measurements and the engine model. It has been demonstrated that the latter leads to lower analysis uncertainty for the high pressure components who are the primary lever for improvements on SFC and EGT-margin. This is explained by the improved accuracy achieved with averaging multiple snapshots. It has been demonstrated that using an average of 50 filtered snapshots is a valid approach, since the engine components may be considered to be a system of constant state during the operation time frame. Furthermore, the importance of the proper choice of the core flow analysis method has been demonstrated, as well as the potential for analysis accuracy improvement using a more detailed engine model. It has been shown that these measures have the potential of improving the analysis accuracy of HPC and HPT by a factor of 1.4 and 3.4 respectively. Analysis of recovered performance of fan and LPT has been demonstrated to be more sensitive to installation effects. For these components, better accuracy can be achieved using test cell data, provided a performance test run is carried out prior to the overhaul.

In order to correlate workscope and performance recovery, a general functional relation has been established to serve as the principal model. The model was then adapted to optimally fit available field data from past engine overhauls through implementation within an appropriate optimisation algorithm. An application to the high pressure components provided sensible results indicating clear distinctions between the leverage that different workscope elements provide for recovering performance. A cross validation using the leave one out algorithm showed the results of the correlation to be sensible. The need for further improvement, for example by using measured dimension changes of the different features for the workscope description, has been demonstrated. With this investigation, it has been understood for the first time what the feasibilities and limitations in correlating workscope and performance recovery are. The established approach provides a basis for systems aimed at systematically planning engine worksopes with respect to performance restoration.

## 7.2 Outlook

The use of more precise hardware data for the hardware's feature state definition provides room for an improved correlation of overhaul actions and their effect. Given the lower number of optimisation parameters needed for such a correlation, this would also allow for the model to be set up with more detail. A clustering of two stages



each for the HPC instead of a front and rear part would be such an increase in detail. The deployment of the necessary processes for an enhanced data collection is foreseeable for the near future, due to a higher degree of automation in measuring and data recording.

Furthermore, performance recovery analysis with optimisation techniques presents a possible field of investigation should an increase in the number of snapshots taken during different flight phases become a new trend in future engine monitoring. The prospect of an improvement of observability with using multiple operating point analysis is of particular interest for the low pressure components, where analysis uncertainty is highest.

The integration of the performance model for the engine overhaul in a comprehensive model would allow for studies of an optimised workscope planning. The enhanced performance model could be integrated with existing methodologies modelling the aspects of scheduling, reliability and cost of engine overhauls. A possible extension to the performance model could be realised with a prognosis model, so as to further minimise SFC during operation and maximise on-wing time.



# Bibliography

- [1] ASTM International. *Standard Specification for Aviation Turbine Fuels, ASTM-D1655-12a*.
- [2] R. B. Abernethy et al. *HANDBOOK - UNCERTAINTY IN GAS TURBINE MEASUREMENTS: AEDC-TR-73-5*. Arnold Air Force Station and Tennessee, 1973.
- [3] D. Agarwal. *John Leahy reveals Airbus A320 NEO (new engine option) plans - Bangalore Aviation*. Ed. by Bangalore Aviation. checked on August 22nd 2012. URL: <http://www.bangaloreaviation.com/2010/11/john-leahy-reveals-airbus-a320-neo-new.html>.
- [4] V. Alatortsev and M. Gumerov H. Alatortsev. "EFFECT OF SERIAL MANUFACTURING PROCEDURES ON FORMING RELATIONSHIPS BETWEEN THERMOGASDYNAMIC PARAMETERS IN GAS TURBINE ENGINES: AIAA-2000-371". In: *36th AIAA/ASME/SAE/ASEE Joint Propulsion Conference and Exhibit*. Ed. by AIAA. 2000.
- [5] American Society of Mechanical Engineers. *Test Uncertainty - Instruments and Apparatus, PTC 19.1-1998*. New York, December 31st 1998.
- [6] K. Bammert, H. Kläukens, and D. Hartmann. "Der Einfluß des radialen Schaufelpalts auf den Wirkungsgrad mehrstufiger Turbinen". In: *VDI-Zeitung* Vol. 10 (1968), pp. 390–395.
- [7] M. Bauer. *Leistung und Systeme von Luftfahrtantrieben: VL17: Engine Condition & Health Monitoring, Engine Condition & Health Monitoring : Lecture TU Berlin*. March 18th 2010.
- [8] F. Beichelt. *Stochastik für Ingenieure*. 1st ed. Stuttgart: Teubner, 1995. ISBN: 3-519-02987-1.
- [9] G. A. Bobula and R. A. Lottig. *INLET REYNOLDS NUMBER AND TEMPERATURE EFFECTS ON THE STEADY-STATE PERFORMANCE OF A TFE731-2 TURBOFAN ENGINE: NASA TM X-3537*. Cleveland, 1977.

- 
- [10] G. E. P. Box, W. G. Hunter, and J. S. Hunter. *Statistics for experimenters: An introduction to design, data analysis, and model building*. 1st ed. New York: Wiley, 1978. ISBN: 0-471-09315-7.
- [11] Australian Transport Safety Bureau. *Engine Failure involving Airbus A380, A6-EDA: AO-2012-150*. Canberra, 2013.
- [12] CFM. *Flight Operations Support*. Training seminar. September 10th 2005. URL: [http://www.smartcockpit.com/aircraft-ressources/CFM\\_Flight\\_Ops\\_Support\\_A320.html](http://www.smartcockpit.com/aircraft-ressources/CFM_Flight_Ops_Support_A320.html).
- [13] D. E. Caguiat. “ROLLS ROYCE/ALLISON 501-K GAS TURBINE ANTI-FOULING COMPRESSOR COATINGS EVALUATION: GT-2002-30261”. In: *Proceedings of the ASME Turbo Expo 2002*. Ed. by ASME. New York: ASME, 2002.
- [14] J. Cheng and M. J. Druzdzal. “Latin hypercube sampling in Bayesian networks”. In: *Proceedings of the Thirteenth International Florida Artificial Intelligence Research Society Conference (FLAIRS-2000)*. Ed. by J. Etheredge and B. Manaris. AAAI Press, 2000.
- [15] O. Córdoba. “GAS PATH ANALYSIS STUDY FOR OVERHAUL ENGINES: GT2005-68137”. In: *Proceedings of the ASME Turbo Expo 2005*. Ed. by ASME. New York: ASME, 2005.
- [16] Deutsches Institut für Normung. *Thermopaare - Teil 2: Grenzabweichungen der Thermospannungen, DIN EN 60584 Part 2*. 1993.
- [17] C. Eichler. *Instandhaltungstechnik*. 2nd ed. Berlin: VEB Verlag Technik, 1979.
- [18] J. Eitel. *Stat 300 (course material)*. Folsom Lake College, Mathematic Department. 2013.
- [19] “Engine Maintenance: maximising performance and minimising costs”. In: *Aircraft Technology Engineering & Maintenance: The MRO Yearbook 2009* (2009), pp. 68–73.
- [20] R. Fiola. *Berechnung des instationären Betriebsverhaltens von Gasturbinen unter besonderer Berücksichtigung von Sekundäreffekten*. Technische Universität München, Institut für Luft- und Raumfahrt, Lehrstuhl für Flugantriebe, Doctoral Dissertation. 1993.
- [21] Forbes Insights, ed. *Forbes Insights: 2011 Global Aerospace Outlook*. 2011. URL: [http://images.forbes.com/forbesinsights/StudyPDFs/CIT\\_Aerospace\\_2011.pdf](http://images.forbes.com/forbesinsights/StudyPDFs/CIT_Aerospace_2011.pdf).

- [22] M. Gerth-Noritzsch. *Untersuchungen zum Betriebsverhalten eines zivilen Strahltriebwerkes*. Technische Universität Dresden, Diploma Thesis. 2011.
- [23] A. Giebmanns et al. "ANALYZING AND OPTIMIZING GEOMETRICALLY DEGRADED TRANSONIC FAN BLADES BY MEANS OF 2D AND 3D SIMULATIONS AND CASCADE MEASUREMENT: GT2012-69064". In: *Proceedings of the ASME Turbo Expo 2012*. Ed. by ASME. New York: ASME, 2012.
- [24] H. Gränicher. *Messung beendet - was nun? Einführung und Nachschlagewerk für die Planung und Auswertung von Messungen*. 2nd ed. Zürich and Stuttgart: Vdf, Hochsch.-Verl. an der ETH Zürich and Teubner, 1996. ISBN: 3-7281-2258-0.
- [25] H. Grieb and Hubert Grieb. *Projektierung von Turboflugtriebwerken*. 1st ed. Basel: Birkhäuser Verlag, 2004. ISBN: 3764360232.
- [26] H. Hart, W. Lotze, and E.-G. Woschni. *Messgenauigkeit*. 2nd ed. Messtechnik. Berlin: Verl. Technik, 1989. ISBN: 3-341-00753-9.
- [27] R. C. Hendricks et al. "FUTURE FUEL SCENARIOS AND THEIR POTENTIAL IMPACT TO AVIATION: 139-ISROMAC-11". In: *ISROMAC-11 Proceedings of the Eleventh International Symposium on Transport Phenomena and Dynamics of Rotating Machinery*. Ed. by Knox Millsaps. o.O.: Curran Associates, Inc., 2006. ISBN: 9781604236774.
- [28] D. Hirndorf. *Einsatz von Optimierungsverfahren in der Leistungsberechnung von Flugtriebwerken*. Technische Universität München, Lehrstuhl für Flugantriebe, Diploma Thesis. 2009.
- [29] Jörg Hoffmann. *Taschenbuch der Messtechnik: Mit 62 Tabellen*. 4th ed. München: Fachbuchverl. Leipzig im Carl Hanser Verl., 2004. ISBN: 3-446-22860-8.
- [30] S. Jessop, S. Valentine, and M. Dr. Roemer. "CBM INTEGRATED MAINTENANCE SCHEDULER: GT2008-51375". In: *Proceedings of the ASME Turbo Expo 2008*. Ed. by ASME. New York: ASME, 2008.
- [31] F. Kappei. *Verbesserung der Analyse des Höhenverhaltens des Niederdruckturbinenwirkungsgrades bei Turboflugtriebwerken*. Universität Stuttgart, Institut für Luftfahrtantriebe, Doctoral Dissertation. 2007. ISBN: 978-3-86624-287-6.
- [32] H.-P. Kau. *Flugantriebe I und Gasturbinen*. Technische Universität München, Lehrstuhl für Flugantriebe, Course Notes. 2005.
- [33] J. C. Kimball. "Improved Gas Turbine Engine Maintenance through Management and Analysis of Engine Performance Data: AIAA-80-1085". In: *16th AIAA/SAE/ASME Joint Propulsion Conference*. Ed. by AIAA. 1980.

- 
- [34] G. J. Kissel. “Rain and Hail Extremes at Altitude: AIAA-79-0539”. In: *Proceedings of the AIAA/SAE 15th Annual Meeting and Technical Display*. Ed. by AIAA. New York: AIAA, 1979.
- [35] Alexander Klötzer. *Untersuchungen zum Betriebsverhalten gemischter Abgassysteme in Luftstrahltriebwerken unter Höhenbedingungen*. Universität Stuttgart, Institut für Luftfahrtantriebe, Doctoral Dissertation. 2012. ISBN: 978-3-86624-568-6.
- [36] J. Kurzke. “CALCULATION OF INSTALLATION EFFECTS WITHIN PERFORMANCE COMPUTER PROGRAMS”. In: *Steady and Transient Performance Prediction of Gas Turbine Engines: AGARD-LS-183*. Neuilly-sur-Seine: North Atlantic Treaty Organization, Advisory Group for Aerospace Research and Development, 1992. ISBN: 92-835-0674-X.
- [37] J. Kurzke. *GasTurb 12: Design and Off-Design Performance of Gas Turbines: Manual*. 2012.
- [38] J. Kuschke et al. “Assessment of In-Service Measurement Uncertainty and its Impact on Performance Recovery Analysis of Overhauled Civil Turbofan Engines: ISABE-2013-1325”. In: *21st International Symposium on Air Breathing Engines*. 2013.
- [39] J. Kuschke et al. “Assessment of Modelling Uncertainties Impact on Performance Recovery Analysis of Overhauled Civil Turbofan Engines: ISABE-2013-1330”. In: *21st International Symposium on Air Breathing Engines*. 2013.
- [40] D. Lawicki. *Jet Fuel Characteristics*. May 2002 URL: [http://www.smartcockpit.com/download.php?path=docs/&file=Jet\\_Fuel\\_Characteristics.pdf](http://www.smartcockpit.com/download.php?path=docs/&file=Jet_Fuel_Characteristics.pdf).
- [41] J. D. MacLeod and J. C. G. Capt Laflamme. “THE EFFECTS OF A COMPRESSOR REBUILD ON GAS TURBINE ENGINE PERFORMANCE: FINAL RESULTS: AGARD-CP-461”. In: *Proceedings of the 68th AGARD Meeting of the Structures and Materials Panel*. Ed. by AGARD. AGARD, 1989, pp. 3–1 –3–13.
- [42] J. D. MacLeod and B. Orbanski. “Turbine Rebuild Effects on Gas Turbine Performance: 92-GT-23”. In: *Proceedings of the ASME International Gas Turbines and Aeroengine Congress and Exposition*. Ed. by ASME. New York: ASME, 1992.
- [43] R. S. Merkler. *Modellierung des Kühlluftsystems von Turboluftstrahltriebwerken im Rahmen von Leistungssyntheseprogrammen*. Universität Stuttgart, Institut für Luftfahrtantriebe, Diploma Thesis. 2003.

- 
- [44] Gerhard Merziger. *Formeln + Hilfen zur höheren Mathematik*. 4th ed. Springer: Binomi, 2001. ISBN: 392392335X.
- [45] C. Moll. *Kennwertermittlung und Systemanalyse des thermo-mechanischen Verhaltens von Turbomaschinenkomponenten*. Universität Stuttgart, Institut für Luftfahrtantriebe, Doctoral Dissertation. 2005.
- [46] A. W. Moore. *Cross-validation for detecting and preventing overfitting*. Lecture. downloaded on June 20th 2013. URL: <http://www.autonlab.org/tutorials/overfit.html>.
- [47] M. Morini et al. "Influence of Blade Deterioration on Compressor and Turbine Performance: GT2008-50043". In: *Proceedings of the ASME Turbo Expo 2008*. Ed. by ASME. New York: ASME, 2008.
- [48] M. H. Müller. *Untersuchungen zum Einfluss der Betriebsbedingungen auf die Schädigung und Instandhaltung von Turboluftstrahltriebwerken*. Universität Stuttgart, Institut für Luftfahrtantriebe, Doctoral Dissertation. 2013.
- [49] H. G. Münzberg and J. Kurzke. *Gasturbinen - Betriebsverhalten und Optimierung*. 1st ed. Springer Verlag, 1976. ISBN: 978-3-540-08032-9.
- [50] Annette Nielsen. *Experimentelle Untersuchungen zum thermischen Verhalten von Turboluftstrahltriebwerken*. Universität Stuttgart, Institut für Luftfahrtantriebe, Doctoral Dissertation. 2006. ISBN: 3-86624-136-4.
- [51] Oxford Economics, ed. *Oil price outlook to 2030*. June 2010. URL: <http://www.oxfordeconomics.com/publication/download/214140>.
- [52] W. H. Press. *Numerical recipes: The art of scientific computing*. 3rd ed. Cambridge, UK, and New York: Cambridge University Press, 2007. ISBN: 978-0-521-88407-5.
- [53] Princeton University, ed. *Interpreting Regression Output*. last checked on August 11th 2014. URL: [http://dss.princeton.edu/online\\_help/analysis/interpreting\\_regression.htm](http://dss.princeton.edu/online_help/analysis/interpreting_regression.htm).
- [54] S. S. Rao. *Optimization: Theory and applications*. 1st ed. New York: Wiley, 1979. ISBN: 0852267568.
- [55] G. Reitz. *Erstellung und Validierung eines Modells zur Bewertung von Wartungsmaßnahmen an Luftsystemen auf die Effizienz von Flugtriebwerken*. Technische Universität Braunschweig, Institut für Flugantriebe und Strömungsmaschinen, Diploma Thesis. 2012.

- 
- [56] O. Rupp. *Vorhersage von Instandhaltungskosten bei der Auslegung ziviler Strahltriebwerke*. Technische Universität München, Institut für Luft- und Raumfahrt, Lehrstuhl für Flugantriebe, Doctoral Dissertation. 2000.
- [57] SAE. *AIR DATA COMPUTER - MINIMUM PERFORMANCE STANDARD, SAE-AS8002, Aerospace Standard AS8002, Revision September 1996*. October 1981.
- [58] G. P. Sallee. *PERFORMANCE DETERIORATION BASED ON EXISTING (HISTORICAL) DATA: JT9D JET ENGINE DIAGNOSTICS PROGRAM: NASA CR-135448*. Ed. by NASA Lewis Research Center. Cleveland, 1978.
- [59] G. P. Sallee, H. D. Kruckenberg, and E. H. Toomey. *ANALYSIS OF TURBOFAN ENGINE PERFORMANCE DETERIORATION AND PROPOSED FOLLOW-ON TESTS: NASA CR-134769*. Ed. by NASA Lewis Research Center. Cleveland, 1975.
- [60] H. Saravanamuttoo. *RECOMMENDED PRACTICES FOR MEASUREMENT OF GAS PATH PRESSURES AND TEMPERATURES FOR PERFORMANCE ASSESSMENT OF AIRCRAFT TURBINE ENGINES AND COMPONENTS: AGARD-AR-245*. Ed. by Advisory Group for Aerospace Research North Atlantic Treaty Organization and Development. Neuilly-sur-Seine, 1990.
- [61] O. Sasahara. “JT9D ENGINE/MODULE PERFORMANCE DETERIORATION RESULTS FROM BACK TO BACK TESTING: ISABE 85-7061”. In: *7th International Symposium on Air Breathing Engines*. 1985, pp. 528–535.
- [62] F. Schirmeister. *Untersuchungen zum Einfluss der Betriebsbedingungen auf die Leistungsverschlechterung von Turboluftstrahltriebwerken*. Universität Stuttgart, Institut für Luftfahrtantriebe, Doctoral Dissertation. 2013. ISBN: 978-3-8439-0937-2.
- [63] L. Schönwälder. *Performancebasierte Kostenoptimierung bei Fan Blade-Reparaturen*. Reihe Realwissenschaften. Saarbrücken: AV Akademikerverlag GmbH & Co. KG, 2012. ISBN: 978-3-639-40072-4.
- [64] J. F. Seaman and I. E. Allen. “Group Effort - Cluster analysis applied in more disciplines to find answers”. In: *Quality Progress* Vol. 46 (2013), pp. 56–59.
- [65] S. Spieler. *Untersuchung zur Leistungsverschlechterung von Turboluftstrahltriebwerken*. Universität Stuttgart, Institut für Luftfahrtantriebe, Doctoral Dissertation. 2009.



- [66] S. Spieler et al. "Probabilistic Engine Performance Scatter and Deterioration Modeling: GT2007-27051". In: *Proceedings of the ASME Turbo Expo 2007*. Ed. by ASME. New York: ASME, 2007.
- [67] G. Spur. *Fabrikbetrieb: Das System, Planung/Steuerung/Organisation, Information/Qualität, die Menschen*. München and Wien: Hanser, 1994. ISBN: 3446177140.
- [68] Staudacher. *Untersuchungen zum sekundären Luftsystem von Luftstrahltriebwerken*. Technische Universität München, Institut für Luft- und Raumfahrt, Lehrstuhl für Flugantriebe, Doctoral Dissertation. 1995.
- [69] *VDI-Wärmeatlas: Berechnungsblätter für den Wärmeübergang*. 8th ed. Berlin: Springer, 1997. ISBN: 3-540-62900-9.
- [70] J. Vatn, P. Hokstad, and L. Bodsberg. "An overall model for maintenance optimization". In: *Reliability Engineering and System Safety* Vol. 51(3) (1996), pp. 241–257.
- [71] J. P. Vlegher. *Measurement Uncertainty Within the Uniform Engine Test Program: AGARD-AG-307*. Ed. by Advisory Group for Aerospace Research North Atlantic Treaty Organization and Development. Neuilly-sur-Seine, 1989.
- [72] P. P. Walsh and P. Fletcher. *Gas Turbine Performance*. 2nd ed. Blackwell Science Ltd., 2004. ISBN: 063206434X.
- [73] M. Wärja and P. Slottner. "CUSTOMER ADAPTED OPTIMIZED MAINTENANCE PLAN FOR GAS TURBINES: GT2007-27706". In: *Proceedings of the ASME Turbo Expo 2007*. Ed. by ASME. New York: ASME, 2007.
- [74] C. Werner-Spatz. *Analysis of Geometry Influences on Aircraft Engine Compressor Performance*. ANSYS Conference & 29th CADFEM Users' Meeting 2011. Stuttgart, October 19th-21st 2011.
- [75] D. Wirth. *Development and Validation of a Customer Bleed Air Model for Civil Aircraft Engines*. Technische Universität Darmstadt, Fachgebiet Gasturbinen, Luft- und Raumfahrtantriebe, Master's Thesis. 2001.
- [76] *Worldwide Market Forecast For Commercial Air Transport 2011-2030: YGR-5073*. 2011. URL: <http://www.jadc.or.jp/wmf11.pdf>.
- [77] R. H. Wulf. *ENGINE DIAGNOSTICS PROGRAM CF6-50 ENGINE PERFORMANCE DETERIORATION: NASA CR-159867*. Ed. by NASA Lewis Research Center. Cleveland, 1980.

- [78] A. J. Yetter. *Why Do Airlines Want and Use Thrust Reversers? A compilation of airline industry responses to a survey regarding the use of thrust reversers on commercial transport airplanes: NASA TM-109158*. Ed. by NASA Langley Research Center. Hampton, 1995.

# Appendix A

## A.1 Ratio of Pressure Measurements Uncertainties

For an indirect Mach number measurement  $M = f(p_s, p, \kappa)$ , the random measurement uncertainty is given by the law of error propagation:

$$\begin{aligned}\sigma_M &= \sqrt{\left(\frac{\partial M}{\partial p} \cdot \sigma_p\right)^2 + \left(\frac{\partial M}{\partial p_s} \cdot \sigma_{p_s}\right)^2 + \left(\frac{\partial M}{\partial \kappa} \cdot \sigma_\kappa\right)^2} \\ &\approx \sqrt{\left(\frac{\partial M}{\partial p} \cdot \sigma_p\right)^2 + \left(\frac{\partial M}{\partial p_s} \cdot \sigma_{p_s}\right)^2}.\end{aligned}\tag{A.1}$$

The impact of uncertainty in  $\kappa$  is negligible given the small uncertainty at typical cruise ambient conditions [72]. The uncertainty of  $\kappa$  per degree temperature measurement uncertainty is 0.00002. The stochastic part of the remaining systematic measurement uncertainty is established analogously:

$$\sigma_{sys,M} \approx \sqrt{\left(\frac{\partial M}{\partial p} \cdot \sigma_{sys,p}\right)^2 + \left(\frac{\partial M}{\partial p_s} \cdot \sigma_{sys,p_s}\right)^2}.\tag{A.2}$$

The ratio of the stochastic part of the remaining systematic measurement uncertainty

and random measurement uncertainty, defined in equation 5.18, then becomes:

$$\lambda \approx \frac{\sqrt{\left(\frac{\partial M}{\partial p} \cdot \sigma_{sys,p}\right)^2 + \left(\frac{\partial M}{\partial p_s} \cdot \sigma_{sys,p_s}\right)^2}}{\sqrt{\left(\frac{\partial M}{\partial p} \cdot \sigma_p\right)^2 + \left(\frac{\partial M}{\partial p_s} \cdot \sigma_{p_s}\right)^2}} \quad . \quad (\text{A.3})$$

With the ratio for the pressure measurements,  $\lambda'$ , defined analogously to equation 5.18, one then obtains:

$$\begin{aligned} \lambda &\approx \lambda' \frac{\sqrt{\left(\frac{\partial M}{\partial p} \cdot \sigma_p\right)^2 + \left(\frac{\partial M}{\partial p_s} \cdot \sigma_{p_s}\right)^2}}{\sqrt{\left(\frac{\partial M}{\partial p} \cdot \sigma_p\right)^2 + \left(\frac{\partial M}{\partial p_s} \cdot \sigma_{p_s}\right)^2}} \\ &\approx \lambda' \quad . \end{aligned} \quad (\text{A.4})$$

## A.2 Uncertainties of Performance Recovery Analysis

### On-Wing Data

Core flow analysis method	$U_{95}$ [%]									
	Fan		Booster		HPC		HPT		LPT	
	$\eta$	$w_{red}$	$\eta$	$w_{red}$	$\eta$	$w_{red}$	$\eta$	$w_{red}$	$\eta$	$w_{red}$
Booster capacity	1.00	0.69	1.41	-	0.09	0.46	0.15	0.32	0.74	0.49
HPT capacity	0.58	0.40	1.40	0.46	0.09	0.19	0.13	-	0.32	0.21
LPT capacity	0.65	0.46	1.40	0.78	0.09	0.42	0.29	0.24	-	-

Table A.1:  $U_{95}$  for analysed component performance recovery (with on-wing data) due to measurement uncertainty and used core flow analysis method

Core flow analysis method	$U_{95}$ [%]									
	Fan		Booster		HPC		HPT		LPT	
	$\eta$	$w_{red}$	$\eta$	$w_{red}$	$\eta$	$w_{red}$	$\eta$	$w_{red}$	$\eta$	$w_{red}$
Booster capacity	0.15	0.10	0.00	-	0.00	0.00	0.07	0.02	0.12	0.08
HPT capacity	0.09	0.06	0.00	0.04	0.00	0.04	0.09	-	0.08	0.05
LPT capacity	0.02	0.02	0.00	0.13	0.01	0.13	0.14	0.06	-	-

Table A.2:  $U_{95}$  for analysed component performance recovery (with on-wing data) due to FHV variation and used core flow analysis method

Core flow analysis method	$U_{95}$ [%]									
	Fan		Booster		HPC		HPT		LPT	
	$\eta$	$w_{red}$	$\eta$	$w_{red}$	$\eta$	$w_{red}$	$\eta$	$w_{red}$	$\eta$	$w_{red}$
Booster capacity	3.89	2.68	0.00	-	0.00	0.01	0.37	0.02	1.24	0.83
HPT capacity	3.94	2.72	0.00	0.03	0.00	0.03	0.37	-	1.26	0.84
LPT capacity	2.09	1.44	0.00	1.37	0.11	1.42	1.07	0.94	-	-

Table A.3:  $U_{95}$  for analysed component performance recovery (with on-wing data) due to nozzle exit area variation and used core flow analysis method

Core flow analysis method	$U_{95}$ [%]									
	Fan		Booster		HPC		HPT		LPT	
	$\eta$	$w_{red}$	$\eta$	$w_{red}$	$\eta$	$w_{red}$	$\eta$	$w_{red}$	$\eta$	$w_{red}$
Booster capacity	0.30	0.20	0.00	-	0.00	0.00	0.01	0.00	0.02	0.01
HPT capacity	0.29	0.20	0.00	0.00	0.00	0.00	0.01	-	0.02	0.01
LPT capacity	0.28	0.19	0.00	0.02	0.00	0.02	0.02	0.01	-	-

Table A.4:  $U_{95}$  for analysed component performance recovery (with on-wing data) due to variation of thrust reverser leakage and used core flow analysis method

Core flow analysis method	$U_{95}$ [%]									
	Fan		Booster		HPC		HPT		LPT	
	$\eta$	$w_{red}$	$\eta$	$w_{red}$	$\eta$	$w_{red}$	$\eta$	$w_{red}$	$\eta$	$w_{red}$
Booster capacity	2.97	2.04	0.00	-	0.12	2.25	1.11	1.48	2.03	1.35
HPT capacity	-	-	-	-	-	-	-	-	-	-
LPT capacity	-	-	-	-	-	-	-	-	-	-

Table A.5:  $U_{95}$  for analysed component performance recovery (with on-wing data) due to non-observable booster capacity change and used core flow analysis method

Core flow analysis method	$U_{95}$ [%]									
	Fan		Booster		HPC		HPT		LPT	
	$\eta$	$w_{red}$	$\eta$	$w_{red}$	$\eta$	$w_{red}$	$\eta$	$w_{red}$	$\eta$	$w_{red}$
Booster capacity	-	-	-	-	-	-	-	-	-	-
HPT capacity	4.56	3.15	0.00	3.28	0.18	3.39	1.76	-	3.04	2.03
LPT capacity	-	-	-	-	-	-	-	-	-	-

Table A.6:  $U_{95}$  for analysed component performance recovery (with on-wing data) due to non-observable HPT capacity change and used core flow analysis method

## Test Cell Data

Core flow analysis method	$U_{95}$ [%]									
	Fan		Booster		HPC		HPT		LPT	
	$\eta$	$w_{red}$	$\eta$	$w_{red}$	$\eta$	$w_{red}$	$\eta$	$w_{red}$	$\eta$	$w_{red}$
Booster capacity	0.44	0.31	1.79	-	0.60	0.63	0.38	0.38	0.29	0.19
HPT capacity	0.46	0.32	1.79	0.58	0.62	0.87	0.32	-	0.43	0.28
LPT capacity	0.47	0.33	1.79	0.47	0.61	0.84	0.52	0.47	-	-

Table A.7:  $U_{95}$  for analysed component performance recovery (with test cell data) due to measurement uncertainty and used core flow analysis method

Core flow analysis method	$U_{95}$ [%]									
	Fan		Booster		HPC		HPT		LPT	
	$\eta$	$w_{red}$	$\eta$	$w_{red}$	$\eta$	$w_{red}$	$\eta$	$w_{red}$	$\eta$	$w_{red}$
Booster capacity	0.01	0.01	0.00	-	0.00	0.01	0.45	0.17	0.55	0.37
HPT capacity	0.07	0.05	0.00	0.26	0.02	0.27	0.61	-	0.39	0.26
LPT capacity	0.29	0.20	0.00	0.88	0.07	0.91	0.97	0.42	-	-

Table A.8:  $U_{95}$  for analysed component performance recovery (with test cell data) due to FHV variation and used core flow analysis method

Core flow analysis method	$U_{95}$ [%]									
	Fan		Booster		HPC		HPT		LPT	
	$\eta$	$w_{red}$	$\eta$	$w_{red}$	$\eta$	$w_{red}$	$\eta$	$w_{red}$	$\eta$	$w_{red}$
Booster capacity	0.69	0.47	0.00	-	0.13	2.02	1.18	1.31	1.19	0.79
HPT capacity	-	-	-	-	-	-	-	-	-	-
LPT capacity	-	-	-	-	-	-	-	-	-	-

Table A.9:  $U_{95}$  for analysed component performance recovery (with test cell data) due to non-observable booster capacity change and used core flow analysis method

Core flow analysis method	$U_{95}$ [%]									
	Fan		Booster		HPC		HPT		LPT	
	$\eta$	$w_{red}$	$\eta$	$w_{red}$	$\eta$	$w_{red}$	$\eta$	$w_{red}$	$\eta$	$w_{red}$
Booster capacity	-	-	-	-	-	-	-	-	-	-
HPT capacity	0.96	0.66	0.00	2.75	0.16	2.87	1.73	-	1.65	1.10
LPT capacity	-	-	-	-	-	-	-	-	-	-

Table A.10:  $U_{95}$  for analysed component performance recovery (with test cell data) due to non-observable HPT capacity change and used core flow analysis method

# Curriculum Vitae

## *Personal Information*

---

Name	Jonathan Sebastian Kuschke
Born	June 23rd 1983 in Celle, Germany
Citizenship	German

## *Work*

---

Since Jan '14	Senior Consultant at Kemény, Boehme & Company, Munich
Jan '10 - Sep '13	System engineer engine performance and doctoral candidate at MTU Aero Engines, Munich
Mar '09 - Aug '09	Diploma Thesis at MTU Aero Engines, Munich
Oct '08 - Feb '09	Working Student at MTU Aero Engines, Munich
Jul '08 - Sep '08	Internship at Rolls-Royce Deutschland, Dahlewitz
Jun '08 - Jul '08	Internship at EADS Military Air Systems, Manching
Jun '07 - Aug '07	Internship at EADS Military Air Systems, Manching
Aug '04 - Sep '04	Internship at August Prien Bauunternehmung, Hamburg

## *Academic Education*

---

Oct '05 - Sep '09	TU München & Supaero Toulouse, double graduate degree in aeronautics & graduate degree in engineering management
Oct '03 - Sep '05	TU Dresden, undergraduate degree in mechanical engineering
Aug '00 - Jun '02	Ricarda-Huch-Gymnasium, Hanover, baccalaureate
Aug '99 - Jun '00	Montgomery County & Bath County, Kentucky, high school graduation